The authors would like to thank both reviewers for their helpful comments. Below we address each comment in turn, starting with reviewer #1. Our responses are highlighted in bold.

Response to comments by Reviewer #1

Major comments:

1. A close reading of Bretherton et al (2007, section 3, paragraph 7) reveals that each of their simulations proceeded identically without sedimentation for two hours before sedimentation was enabled in two of the three simulations. My impression is that the initial absence of turbulence and convection in the boundary layer allows the presence/absence of sedimentation to have an outsize effect when there is no compensating water flux into the inversion. With a cloud droplet sedimentation speed of 5 mm/s (which seems about right for qc=0.5g/kg and Nd=500/cm3), the cloud layer would subside by one grid level (10m) over 2000 seconds, or about a half hour. If it takes the turbulence about a half hour to spin up at the start of the simulation, this sedimentation might account for a significant part of the difference in inversion height between CASIM_NO_PROC and SIMPLE_CLOUD at 0530, which I estimate as 20m. Isolating the effect of sedimentation by turning on/off sedimentation in an already turbulent boundary layer would eliminate this uncertainty and strengthen the study in my view.

For the present paper, I would suggest using the CASIM_NO_PROC simulation as the control for the first two hours since it does a good job of maintaining the observed LWP and then branching all the simulations from that point. If it's easier, use CASIM_NO_SED in place of SIMPLE_CLOUD since the restart file may not want the microphysics scheme to be switched. If the comparisons of early morning cloud and boundary layer properties should stay at 0530 hours, perhaps the start of the spin-up simulation should be pushed back to 0130 hours.

Perhaps, this won't have a huge effect, but it's worth checking.

We have followed the reviewer's advice by re-running the test simulation with sedimentation disabled within an already turbulent boundary layer. This was achieved by first re-running the CASIM_NO_PROC simulation to generate a checkpoint restart file after 90 minutes of simulation time (the time taken for the model to spin-up from the initial conditions, based on a timeseries plot of the maximum vertical velocity within the domain; see Figure below). The model was then restarted from this 90 minute checkpoint file, but with sedimentation turned off whilst all other settings were kept the same, to produce the new CASIM_NO_SED experiment.

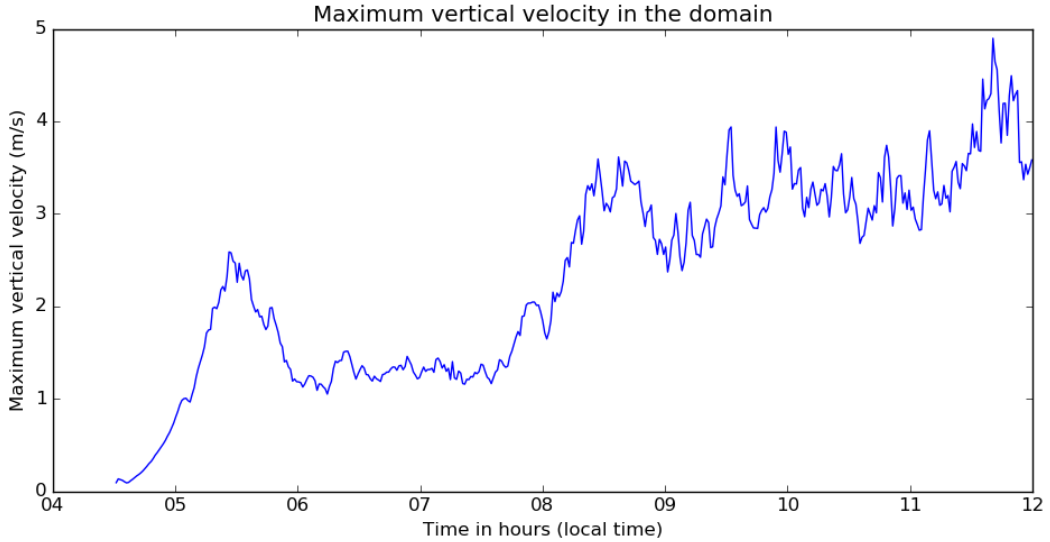

To assess the impact on our results, we have reproduced some key plots from the original manuscript, replacing SIMPLE_CLOUD with CASIM_NO_SED. The findings are summarised as follows.

Regarding the comparison with liquid water path (LWP) observations, the new CASIM_NO_SED simulation still underestimates the variability in LWP between 0530 and 0700 hours compared to the observations at Save (see figure below), as was the case with SIMPLE_CLOUD (cf figure 10 in the original manuscript).

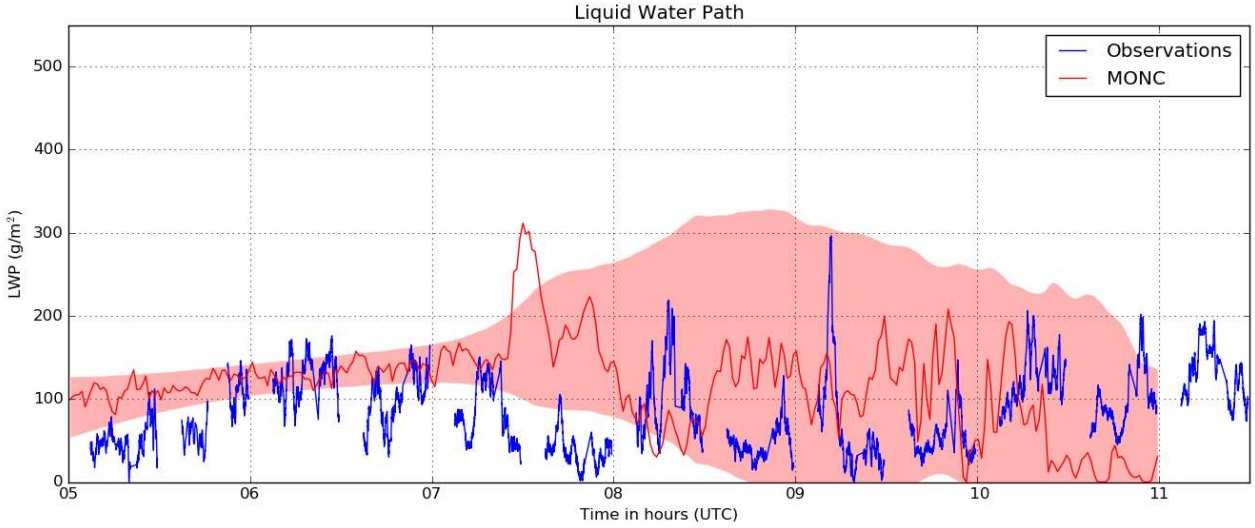

Comparison of LWP timeseries at Savé from 5 July 2016 (blue) as measured by the microwave radiometer (Wieser et al., 2016), with simulated LWP from CASIM_NO_SED, showing the evolution of LWP at the centre of the model domain (red line) and the LWP variability within the whole domain (red shading), expressed as +/- 2 standard deviations from the domain mean value.

The plot below compares the timeseries of the mean LWP in the domain for both CASIM_NO_PROC and CASIM_NO_SED. The trend in CASIM_NO_SED is much the same as it was in SIMPLE_CLOUD (cf Figure 12 in the original manuscript).

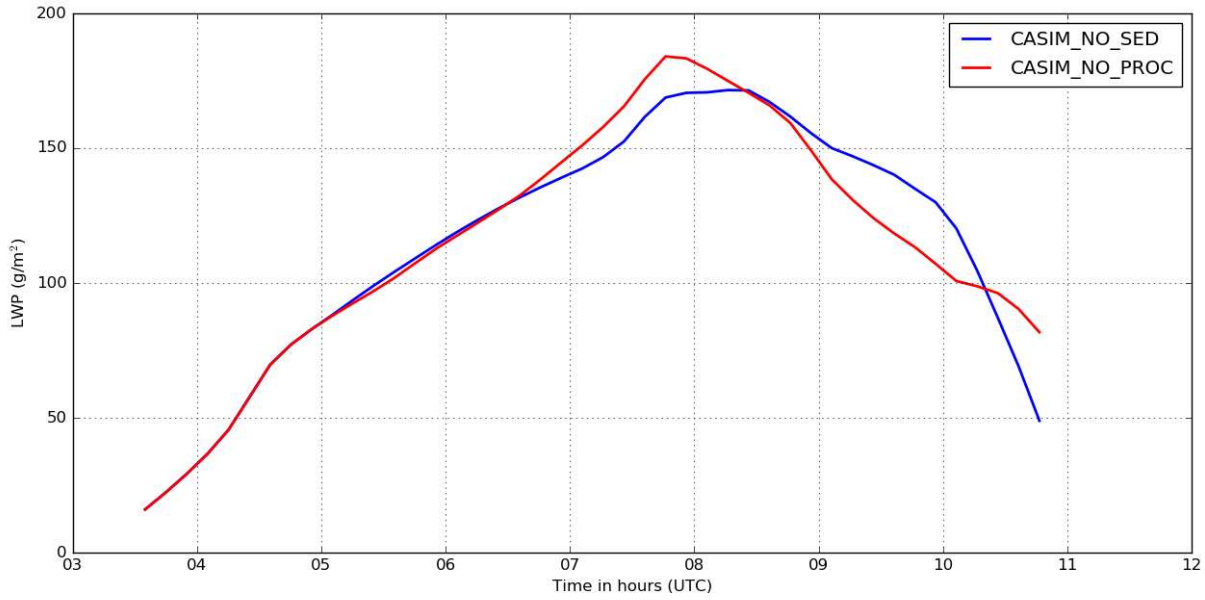

Timeseries of simulated LWP (g m −2) from CASIM_NO_PROC (red) and CASIM_NO_SED (blue)

Finally, the spatial distribution of LWP in CASIM_NO_SED still exhibits the same overly homogeneous structure as SIMPLE_CLOUD relative to CASIM_NO_PROC at 0530 UTC and 0700 UTC, as shown in the plot below (cf Figure 11 in the original manuscript).

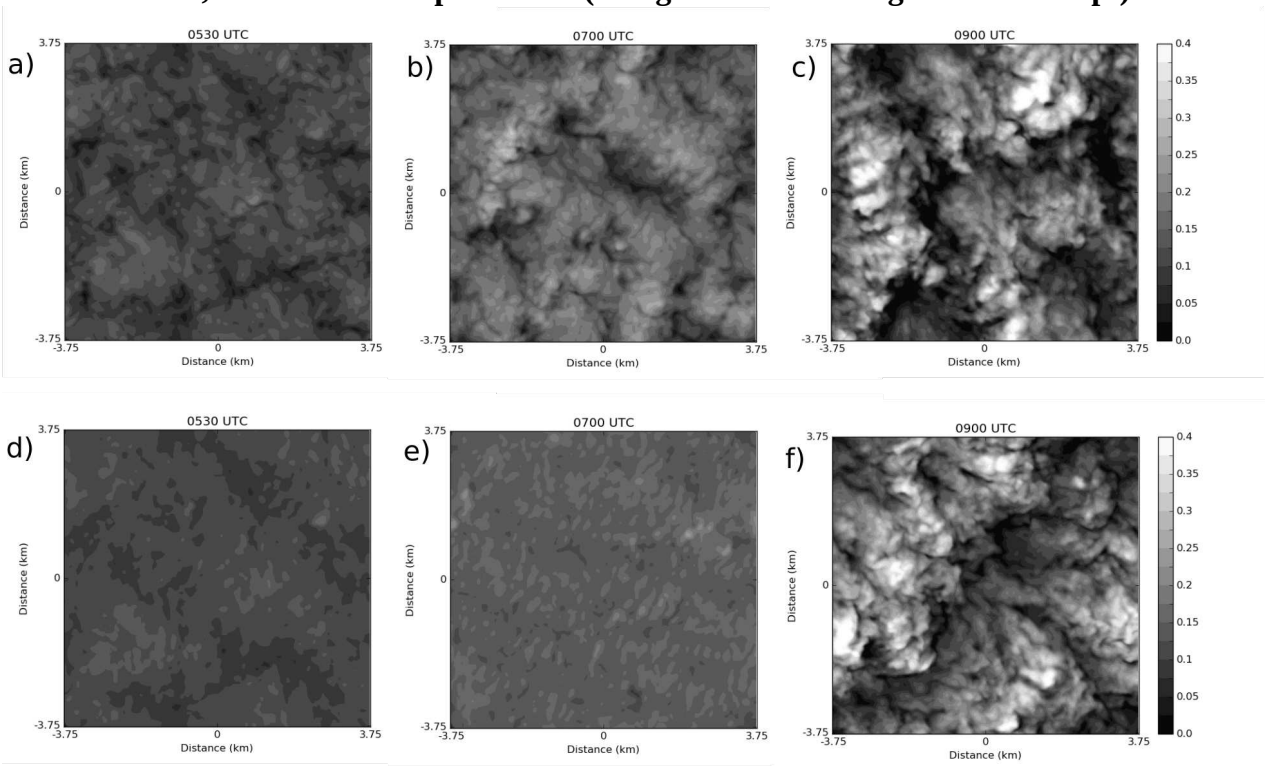

Maps showing the spatial distribution of LWP (kg m −2) within the model domain at 0530, 0700 and 0900 UTC for CASIM_NO_PROC (a-c; top row) and CASIM_NO_SED (d-f; bottom row).

Based on this assessment, we conclude that the suppression of sedimentation during the spin-up of turbulence in the original SIMPLE_CLOUD simulation has negligible impact on our conclusions. Nevertheless, for consistency with Bretherton et al 2007, we have decided to update the manuscript so that we now include results from the new CASIM_NO_SED simulation in the revised manuscript instead of the original SIMPLE_CLOUD test experiment. No changes were made to the CASIM_200, CASIM_100 and CASIM_50 simulations for the revised manuscript.

Note that whilst setting up the CASIM_NO_SED experiment, we also investigated the use of an earlier model start time as suggested by the reviewer. Initialising both CASIM_NO_PROC and CASIM_NO_SED from 0230 UTC rather than 0330 UTC did not have any appreciable impact on the relative difference in LWP between the control and test simulation, but it did result in an overestimation of the liquid water path compared to the observations at around 0500 hours in the control simulation. For this reason, we decided to stick with the original initialisation time of 0330 UTC.

We would also like to point out that by replacing SIMPLE_CLOUD with CASIM_NO_SED, it was necessary to make a number of relatively small changes to the manuscript for consistency, mainly in the Introduction and Model Description sections. With this in mind, we have produced a version of the revised manuscript with track changes, where all differences with respect to the original manuscript are clearly highlighted.

1a. The results of Ackerman et al (2004) suggest that the effect of sedimentation may be more notable in boundary layers with dry air above the PBL. Toll et al (2017, GRL, https://doi.org/10.1002/2017GL075280) note an LWP decrease in ship and volcano tracks in non-precipitating clouds with dry air aloft (bottom of their figure 2) that could be related to the droplet sedimentation effect. It would be interesting to see that same effect here in a boundary layer with a very weak moisture jump across the inversion. The effect on entrainment could be compared to the parameterization in section 6 of Bretherton et al.

The authors agree that it would certainly be interesting to explore the effects of sedimentation in a boundary layer with a weaker moisture jump across the inversion. However, the focus of the present study is on a single DACCIWA case study where the humidity and temperature profiles are constrained from observations. We feel that to perform extra sensitivity simulations of this nature would extend the present study beyond its original scope, and on this basis we feel this would be more appropriate as part of a separate follow-on study.

2. Comparing cloud base observations with simulations: Instead of plotting the time series of a single model column for comparison with the observed cloud base height, I would suggest plotting three quantities than span the range of cloud base heights in the model:
+ the inversion height (roughly the top of the stratocumulus cloud),
+ the median cloud base height of cloudy column (roughly stratocumulus cloud base),
+ the lowest cloud base (where cloud fraction first reaches 1% or so) or the LCL of the subcloud layer. This roughly gives the cumulus cloud base in a decoupled boundary layer.

The observed cloud base height will nicely follow these lines, I think, with the lowest model cloud base capturing the low observed cloud base heights after 1000 hours. The presence of fog makes the computation of the lowest cloud base/LCL a bit more complicated, but I would suggest lowest non-fog cloud base. Note that the divergence of the median cloud base height from the lowest cloud base/LCL is a good indicator of decoupling.

The reviewer implies that we are only plotting the time series of a single model column for comparison against the observed cloud base height, but that is not strictly true. We plot two timeseries from the model – the first is the domain mean cloud base height, and the second is the cloud base height from the column at the centre of the model domain. Together, we feel these two quantities provide a satisfactory representation of the simulated cloud base height and its variation with the model. The main purpose of the Figure is to characterize the representation of cloud base height in the model with respect to the observations, as opposed to diagnosing the coupling state of the boundary layer. As such we feel that including the simulated inversion height in the same plot as well could potentially be confusing to the reader. On balance we have decided to stick with our original approach, but we have also overlaid timeseries plots from CASIM_NO_SED as well, as suggested by reviewer #2.

Minor comments (5/26 means page 5, line 26):

5/1: What time is sunrise? I'm not sure it's crucial, but I felt myself wondering as I read the manuscript.
Sunrise was at 0537 UTC. This is stated in the original manuscript on page 5, line 22.

8/20: Suggested re-wording: "... by virtue of the effect of increased droplet size and excessive sedimentation velocity on entrainment."
Done.

9/30: Suggested re-wording: "... and _possibly_ the circulation of the West African monsoon."
Done.

Figures: These are stylistic suggestions, but I feel that grouping these many figures into fewer multi-panel figures could help the reader interrogate their meaning more easily. Feel free to ignore this advice if you wish.

Thank you for the ideas to help consolidate the figures. We have strived to implement these where possible; see individual responses below.

+ Fig 0: An additional figure with a map-like image would be helpful for the reader who hasn't thought so carefully about clouds over Africa. How about a visible geostationary satellite image from 11Z showing the breakup of the cloud along with the locations of the coast, Save, Lome and the transect?

We have included a new Figure (Figure 1 in the revised manuscript, and reproduced below) showing the 0.6 micron visible channel from the Meteosat-10 geostationary satellite. It reveals the cloud structure over southern West Africa at 1012 UTC on 5th July 2016, with borders and coastlines highlighted along with the locations of Save and Lome, labelled 'A' and 'B' respectively in the figure. Note that the satellite image represents all cloud, not just the low-level cloud, but nevertheless the extent of the cloud cover over the Guinea coast is still evident.

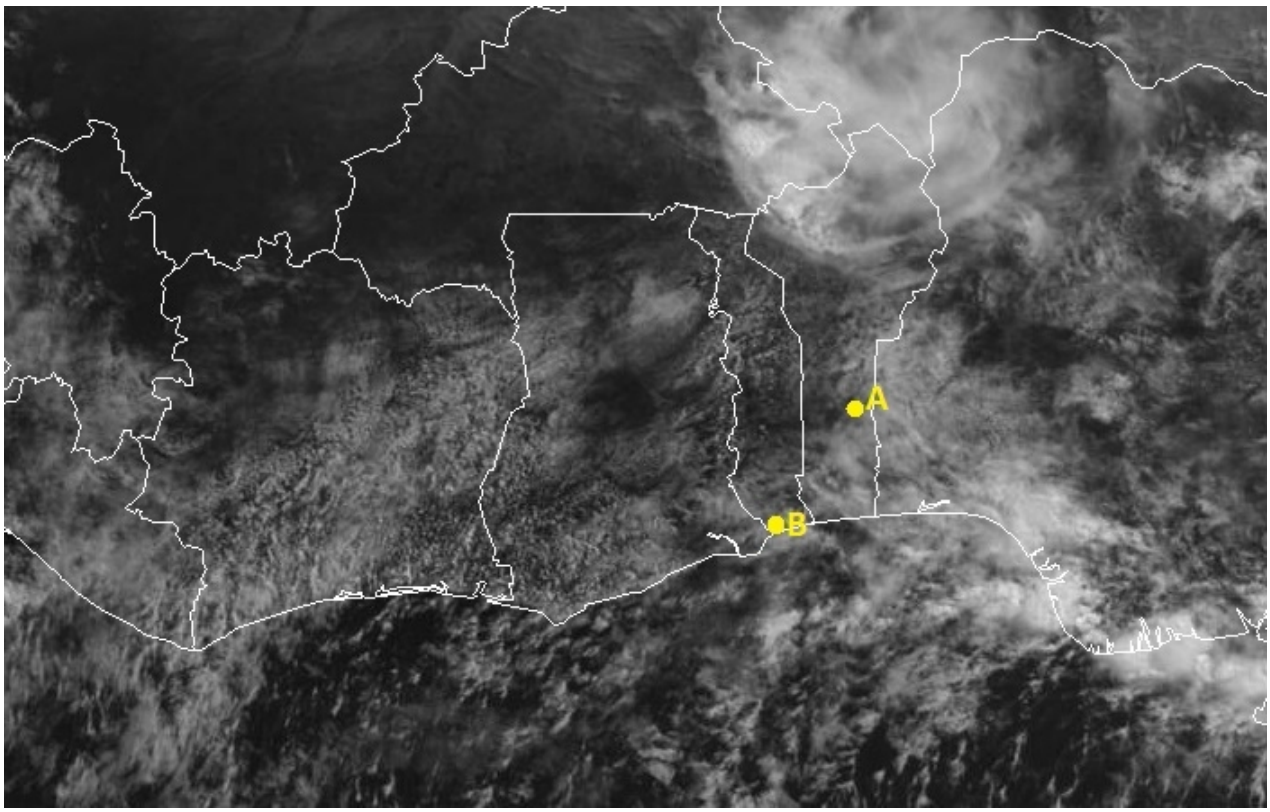

+ Fig 2: A bigger colorscale would be helpful.
It is difficult to enlarge the color scale since it is embedded within the images obtained from the infrared camera and cannot be plotted separately. Instead we have added the following text to the Figure caption: "The images from the camera are coded in RGB colors (red, green, and blue), providing a qualitative estimate of cloud cover during the day and night. The image colour is dependent on the emissivity of the sky and consequently on the brightness temperature, such that red indicates warm and blue cold." We have also made a correction to the reference in the caption – rather than Handwerker et al 2016, it now reads 'Derrien et al 2016'.

+ Figs 3-4: Could figures 3 and 4 be stacked? It would be cool to see Fig 3 extended over the full 24 hours and see the re-formaton of the jet in the evening. This would also let the reader clearly see the result of the strong afternoon surface buoyancy flux on the wind field.
Thanks for this idea; we have stacked the two figures in the revised manuscript as suggested, using an extended x-axis for both plots to show the re-formation of the jet in the evening. The result is shown below:

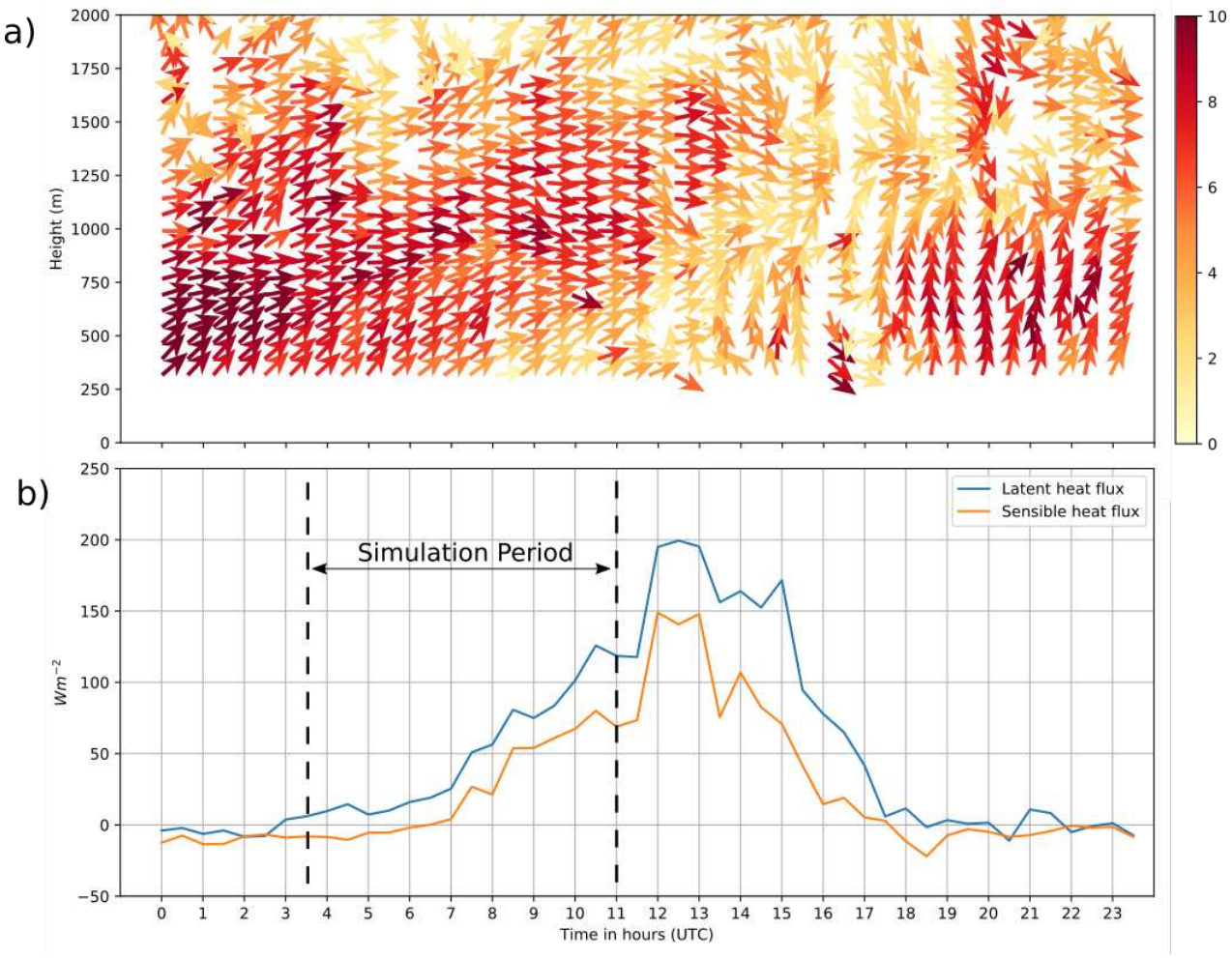

+ Figs 5-6: Could these be stacked?
- Fig 5: I think it would be helpful to NaN (make blank) the regions where qc==0.

Both suggestions above have been incorporated into the revised manuscript, to form the new two-panel Figure 5.

- Fig 6: Note major comment 2 above. If the cloud-free regions are white in figure 5, these lines could even be superimposed on figure 5, though that might be too much.
We chose to keep the cloud base height plots as a separate sub-figure in the end (Figure 5b in the revised manuscript), since we couldn't find an acceptable way to make the lines stand out against the shaded contours in Figure 5a.

+ Figs 7,13: Could these be stacked with an additional panel for the 1100 UTC version of SIMPLE_CLOUD? Could the lowest cloud base, median cloud base and inversion height be marked as dashed lines.
We have stacked Figs 7 and 13, and included the additional panel for the 1100 UTC version of CASIM_NO_SED, as suggested. See Figure 6 in the revised manuscript.

+ Fig 8: If the authors think it's helpful, could the observations from figure 1 be added as dashed lines?
Done; see Figure 7 in the revised manuscript.

+ Figs 9, 10, 16: Could these be stacked as a three-panel figure? I felt the need to flip back and forth to compare the different versions of this figure.
We have stacked the original Figures 9 and 10 as a single figure, to form Figure 8 in the revised manuscript. We have kept the original Figure 16 (now Figure 13) separate, since a three-panel figure made each individual image too small and difficult to read.

+ Figs 12, 15: Could the lines in figure 15 be added as dashed lines in figure 12 if that's not too distracting?
Done; see Figure 10 in the revised manuscript.

Table 1: Could the cloud droplet number concentration be added to the table? For the run with predicted droplet concentration, a range of values could be given that could be different between the two times if appropriate.
Given that CASIM_NO_PROC is the only simulation where the droplet number concentration is predicted, we have decided not to add this information to Table 1. Note that the range of predicted droplet number concentrations is already quoted in the original manuscript (on page 8 line 14).

Response to comments by reviewer #2

Using an observationally well-characterized case in southern West Africa, the role of sedimentation of cloud droplets in determining liquid water path and heights of low-level clouds, once established, is illustrated using large-eddy simulation and microphysical parameterizations with and without sedimentation. Controls by cloud drop number concentration (and drop size) on the extent to which sedimentation is effective in determining cloud height and water path are also discussed.
This is an important paper, extending earlier work on marine clouds and potential cloud-aerosol interactions related to sedimentation to land clouds. Although many questions remain, especially related to the roles of interactive surface fluxes of heat and moisture, which are not considered here, the paper advances knowledge of low-clouds in a region where they play an important role in the regional surface radiation balance and may be subject to strong aerosol interactions.

The paper is generally well written. While I agree with RC 1 about consolidating figures, the study offers the opportunity to illustrate some of the physical mechanisms at play in more detail, and I suggest the authors consider doing so. Specifically:

1. On Fig. 6, characterize the cloud base altitude for SIMPLE_CLOUD as has been done for CASIM_NO_PROC.
As suggested, we have now included timeseries plots from the new CASIM_NO_SED simulation and overlaid these on to Figure 5b in the revised manuscript.

2. A figure illustrating the different mixing ratio profiles for the cases in Table 1 would help to visualize the corresponding differences in sedimentation in these cases. A figure showing some measure of droplet size would also be helpful.
We have given careful consideration to the reviewer's suggestion of adding new figures, both here and in relation to comment #4 below. In light of the overall need to reduce / consolidate the overall number of figures in the manuscript, we have decided not to add additional figures to complement table 1. Instead we have introduced a new figure to quantify the rates of evaporative cooling and longwave radiative cooling, in response to comment #4 below.

3. What are the units of the field shown in Fig. 2?
There is no unit as such for the images from the cloud camera. The color scale is dependent on the emissivity of the sky and, consequently, the brightness temperature, where red colours indicate warm temperatures and blue cold temperatures. The images are used solely to provide a qualitative estimate of the horizontal homogeneity of the cloud deck (see also response to reviewer #1).

4. The importance of long-wave radiative cooling is discussed for three features of the simulation: (1) cloud formation and maintenance (p. 5, ll. 25-28; p. 7, ll. 15-18; p. 9, l. 25); (2) formation of stable layer near surface overnight (pp. 5-6); and (3) reduced long-wave cooling near cloud top due to sedimentation (p. 7, l. 9). Figures illustrating radiative cooling rates would illustrate these points effectively. Also, with sedimentation, both radiative and evaporative cooling are reduced near cloud top. A figure comparing these rates would be very useful in understanding the relative roles of the two processes.

We have re-run simulations of CASIM_NO_PROC and SIMPLE_CLOUD (now replaced with CASIM_NO_SED as discussed in response to reviewer #1) to include additional profile diagnostics of the longwave cooling rate and evaporative cooling rates. We have added an additional figure to the manuscript to compare these rates in both simulations, as shown below:

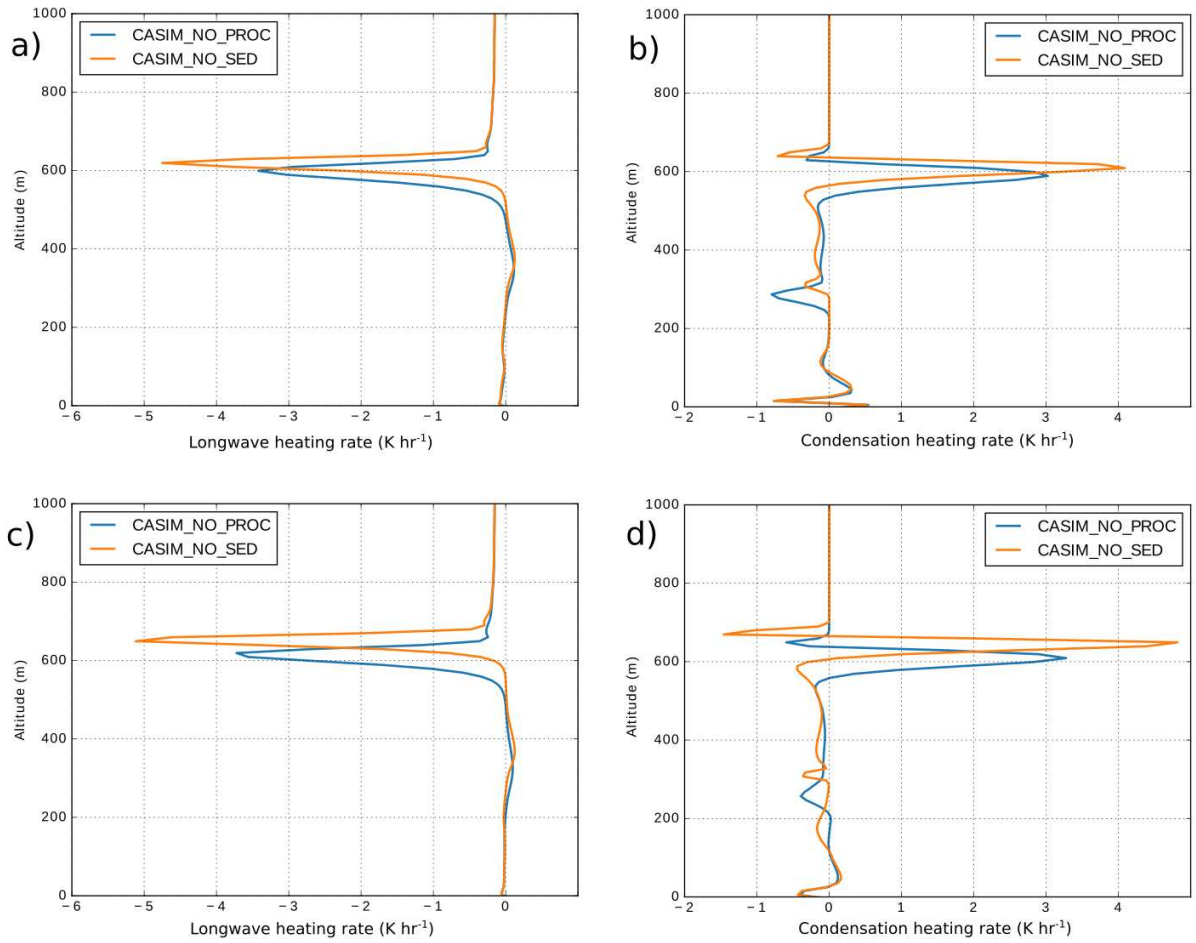

Figure 11. Domain average vertical profiles of a) longwave radiative heating rate (K hr −1) and b) condensation heating rate (K hr −1) calculated as temporal means between 0500-0530 UTC for CASIM_NO_PROC (blue) and CASIM_NO_SED (orange). Longwave and condensation heating rates for the period 0630-0700 UTC are shown in c) and d) respectively.

The following text has also been added to the Results section of the revised manuscript:

"A closer inspection of Fig. 11 reveals more information about the relative roles of radiative cooling and evaporative cooling in the evolution of the cloud layer. In both simulations, it is clear that radiative cooling is the dominant process, with peak rates that are typically an order of magnitude larger than those produced by evaporation near cloud top. The absence of sedimentation in CASIM_NO_SED results in larger cooling rates associated with both processes. However, the increase in longwave cooling rates is relatively modest - around 37% by 0700 UTC - whereas evaporative cooling rates increase by a factor of 2 within the same time period. Thus in relative terms, the effect of sedimentation appears to have the largest impact on rates of evaporative cooling."

The role of droplet sedimentation in the evolution of low level clouds over southern West Africa

Christopher Dearden[1,a], Adrian Hill[2], Hugh Coe[1], and Tom Choularton[1]

[1]Centre for Atmospheric Science, School of Earth and Environmental Science, University of Manchester, United Kingdom
[2]Met Office, Exeter, United Kingdom
[a]now at: Centre of Excellence for Modelling the Atmosphere and Climate, School of Earth and Environment, University of Leeds, United Kingdom

Correspondence to: Christopher Dearden (c.dearden@leeds.ac.uk)

Abstract. Large eddy simulations are performed to investigate the influence of cloud microphysics on the evolution of low level clouds that form over southern West Africa during the monsoon season. We find that, even in clouds that are not precipitating, the size of cloud droplets has a non-negligible effect on liquid water path. This is explained through the effects of droplet sedimentation, which acts to remove liquid water from the entrainment zone close to cloud top, increasing liquid water path. Sedimentation also produces a more heterogeneous cloud structure and lowers cloud base height. Our results imply that an appropriate parameterization of the effects of sedimentation is required to improve the representation of the diurnal cycle of the atmospheric boundary layer over southern West Africa in large-scale models.

1 Introduction

During the months of June to September, the climate of southern West Africa (SWA) is dominated by the southwesterly flow of the West African Monsoon (WAM), which is principally driven by a north-south pressure gradient associated with the Saharan heat low and brings seasonal rains to the region (e.g. Sultan and Janicot 2000, LeBarbé et al. 2002). Clouds, through their diabatic effects, are known to exert an influence on the WAM circulation. For example, a number of studies have explored the role of moist convection in the Sahel (e.g. Garcia-Carreras et al. 2013; Marsham et al. 2013; Birch et al. 2014), revealing that the diurnal cycle of latent heating and cloud radiative forcing affect the north-south pressure gradient and hence the northward advection of moisture.

Low level clouds (LLCs) over SWA, with bases only a few hundred metres above ground level (agl), are also a common occurrence during the WAM season (e.g. Schrage and Fink 2012; van der Linden et al. 2015), yet it is only recently that their role has been considered in detail. LLCs typically form near the Guinea Coast sometime after sunset following the initiation of the southwesterly nocturnal low level jet. The jet is linked to the low-level pressure gradient, supplying moisture to the Sahel region where it is mixed as a result of convection during the day (Parker et al., 2005; Lothon et al., 2008; Abdou et al., 2010;

Bain et al., 2010). The clouds then spread northwards inland during the night (Schuster et al., 2013; van der Linden et al., 2015; Kalthoff et al., 2017), and typically persist until the late morning after which they transition to broken cumulus and dissipate. Through their impact on surface solar irradiance, the LLCs play an important role in the evolution of the atmospheric boundary layer (Gounou et al., 2012), and the regional climate of West Africa (e.g. Knippertz et al. 2011; Hannak et al. 2017).

The most comprehensive observational study of the atmospheric boundary layer over SWA was conducted recently by Kalthoff et al. (2017) during the DACCIWA field campaign (Knippertz et al., 2015a, 2017; Flamant et al., 2017). Between 14 June and 30 July 2016, intensive observations were made at three ground-sites - Savé (Benin), Kumasi (Ghana) and Ile-Ife (Nigeria) - using a variety of instrumentation including infrared cloud cameras, radiosondes and wind profilers (Derrien et al., 2016), radars and ceilometers (Handwerker et al., 2016) and microwave radiometers (Wieser et al., 2016). These ground-based observations were complemented by in-situ measurements of aerosol and cloud properties from three European aircraft, which together conducted 50 research flights between 27 June and 16 July. The results presented in Kalthoff et al. (2017) reveal significant variability in the onset and dissolution of LLCs over southern West Africa from day-to-day and from site-to-site. However the governing processes and mechanisms responsible are not fully understood. Furthermore, large-scale models struggle to represent these LLCs and their variability accurately. Hannak et al. (2017) found that many current GCMs suffer a common bias in the form of insufficient low cloud cover over SWA, abundant solar radiation, and thus too large a diurnal cycle in temperature and relative humidity. They concluded that targeted model sensitivity experiments are needed to test possible feedback mechanisms between low clouds, radiation, boundary layer dynamics, precipitation, and the WAM circulation.

Several studies have proposed specific mechanisms relevant for the formation and break up of the cloud decks (e.g. Schrage and Fink 2012; Schuster et al. 2013; Adler et al. 2017). Specifically, LLCs are believed to be sensitive to temperature and moisture advection from the south (controlled by the strength of the low level jet), vertical mixing of heat and moisture arising due to shear-generated turbulence, radiative cooling at cloud top, condensational heating, sub-cloud evaporation, orographic lifting and lifting induced by gravity wave propagation. In addition to each of these processes, it is important to consider also the role of microphysics in the evolution of LLCs, and the potential modification of the cloud properties via the interaction with aerosols (Knippertz et al., 2015a, b). The combination of ground-based and in-situ measurements from DACCIWA offer a unique opportunity to explore the links between aerosols, microphysics and the bulk cloud properties in SWA, and to inform an appropriate level of parameterization for the representation of LLCs in regional and global models.

~~The~~ One particular microphysical process of interest is the role of droplet sedimentation - the gravitational settling of liquid droplets suspended within the cloud layer. Previous studies of non-drizzling marine stratocumulus have demonstrated that droplet sedimentation has a non-negligible impact on the evolution of liquid water path (LWP) (e.g. Ackerman et al. 2004; Bretherton et al. 2007). However the role of sedimentation in relation to low-level clouds over SWA has not yet been investigated in detail, despite the potential for changes in aerosol properties in the SWA region to modify the size distribution of cloud droplets (and in turn their sedimentation velocity). Hence the purpose of the present study is to ~~address this issue by performing~~ perform large eddy simulations of a selected DACCIWA case study ~~, with a focus on testing~~ to isolate the effects of droplet sedimentation and quantify its impact on the ability of the model to reproduce the observations~~through a consideration of the treatment of the cloud microphysics~~. In doing so, the aim is to identify an optimum configuration for the parameterization

of boundary layer clouds over SWA. The rest of this paper is organised as follows. Section 2 presents details of the case study to be simulated; section 3 describes the numerical model used to perform the simulations, along with details regarding model configuration and initialisation, and the results are presented in section 4. Implications of the findings are discussed in section 5, before the main conclusions are summarised in section 6.

2 Case study

For the purpose of this study, we focus on a particular case on 4th-5th July 2016, the 7th Intensive Observation Period (IOP) from the DACCIWA field campaign (Flamant et al., 2017). The ~~conditions on this day~~ satellite image in figure 1 reveals the extent of the cloud coverage over SWA at 1012 UTC on 5 July 2016. The conditions were fairly typical of the campaign as a whole, with observations collected at the ground site at Savé (labelled 'A' in figure 1) revealing the onset of the low level jet around 1800 UTC on the 4th July, followed by the formation of a low-level stratocumulus deck during the night. Cloud at the Savé ground site was first observed at 0300 UTC on the 5th July, which persisted until around mid-day local time after which it began to break up into patchy cumulus (see Flamant et al. 2017, their Fig.6). No precipitation was recorded at the Savé ground site for this case, consistent with the majority of days sampled during the campaign period. For an overview of the diurnal cycle of the atmospheric boundary layer at Savé during DACCIWA, the reader is referred to Kalthoff et al. (2017).

The radiosonde data from IOP 7 provide more information on the structure and evolution of the boundary layer on this day. Profiles of potential temperature and relative humidity from the 0330 UTC sonde, launched approximately half an hour after the cloud was first detected at Savé, are shown in ~~Fig~~figure 2a-b. The relative humidity profile reveals a cloud layer approximately 200m thick, with a cloud top height of 550m capped by a temperature inversion of 1.5 K. The horizontal wind components, shown separately in ~~Fig~~figure 2c-d, reveal a low level jet with a wind speed maximum at a height of 550m agl, and the cloud layer located directly beneath. Later sondes from 0500, 0628, 0800 and 0928 UTC (not shown) reveal that the cloud layer persisted throughout the morning, with the relative humidity occasionally peaking just below water saturation, suggesting the presence of some breaks in the cloud cover. This is consistent with images from the infrared camera at Savé (see ~~Fig.~~ figure 3), further analysis of which is presented in Dione et al. (2018) over the whole campaign period. The low level jet persisted until around 1100 UTC (~~Fig. ??~~figure 4a), by which time the depth of the boundary layer had increased to 1 km due to solar heating of the surface, resulting in lifting of the cloud deck (as shown in ~~Fig~~figure 2a-b). Three research aircraft were also deployed in sequence on this day, taking in-situ measurements along the transect between Lome (labelled 'B' in figure 1) and Savé from 0800 UTC through to 1800 UTC in order to sample the microphysical evolution during the cloud lifecycle (Flamant et al., 2017).

3 Model description

To fulfill the needs of this study we utilise the Met Office/NERC Cloud model (MONC; Brown et al. 2015). MONC is a re-write of the original Met Office Large Eddy Model (LEM), which has been used extensively over the past twenty years to study

cloud processes in a variety of regimes (e.g. Brown 1999, Brown et al. 2002, Clark et al. 2005, Connolly et al. 2006, Marsham et al. 2006, Connolly et al. 2013, Young et al. 2017). MONC offers several key advantages over the original LEM, including code optimisations, bug-fixes and a new solver that enables simulations to be performed with relatively large domain sizes without having to compromise on the model resolution.

Radiation is represented in MONC by the Suite of Community Radiative Transfer codes based on Edwards and Slingo (SOCRATES; Edwards and Slingo 1996), the same as that used in the Met Office Unified Model, specifically the Global Atmosphere Model 6.0 (Walters et al., 2017). SOCRATES is called on a three minute timestep, allowing the effects of long wave cloud top cooling and short wave absorption within the cloud layer to be captured in the model.

Regarding the treatment of cloud processes, MONC ~~can be~~ is coupled to the CASIM (Cloud-AeroSol-Interacting-Microphysics) module, a newly developed user configurable multi-moment scheme that represents five hydrometeor species (cloud, rain, ice, snow and graupel) and multi-mode aerosols. CASIM has already been used within the Met Office Unified Model to study aerosol-cloud interactions in different meteorological contexts, e.g. Grosvenor et al. (2017), Miltenberger et al. (2017) and Stevens et al. (2017). ~~There is also the option to run MONC using a comparatively basic 'all or nothing' cloud scheme that represents only the effects of condensation and evaporation using a single prognostic variable (the cloud mass mixing ratio). In this scheme, there is no sedimentation of cloud or rain, no autoconversion or accretion, and no aerosol information specified. In the present study , MONC experiments are performed using both CASIM and the simple cloud scheme, with further details~~ Further details on the specific configuration of CASIM used in the present study are given in section 3.2.

3.1 Model initialisation and configuration

MONC is initialised using profiles of potential temperature, total water mass mixing ratio and horizontal wind components, which are obtained from radiosondes launched from the Savé ground site. For IOP 7, we initialise the model using data from the 0330 UTC radiosonde as shown in ~~Fig.~~figure 2, interpolating the data onto the model grid with a vertical resolution of 10 m. Where the initial relative humidity profile is at water saturation (i.e. between 350 m and 550 m in ~~Fig.~~figure 2b), the cloud liquid water mass mixing ratio profile is calculated assuming an adiabatic cloud parcel ascent from cloud base to cloud top. The profile of total water mass mixing ratio is then calculated as the sum of the cloud liquid water and water vapour mass mixing ratios at each model level. During the first model timestep, this supersaturated profile results in the immediate production of a cloud layer via condensation, and at an early enough stage in its lifecycle to study its subsequent evolution over a period of 7.5 hours. The choice of the 0330 UTC sonde for initialisation is justified since the aim of the present study is to focus on the role of microphysical factors that control the subsequent evolution of the LLC, rather than the meteorological factors that govern the onset of cloud formation.

Regarding the forcing of the wind field, the winds from 0330 UTC are relaxed towards the u and v wind components from the 1100 UTC radiosonde (as shown in ~~Fig.~~figure 2c-d) over a period of 7.5 hours. This allows the model to maintain the low level jet throughout the simulation period. No forcing increments are applied to either the potential temperature field or the moisture fields; however a constant large-scale divergence of 5.e-6 s^{-1} is imposed throughout the model domain, to produce a

constant large-scale subsidence. According to the ERA-Interim reanalysis dataset (Dee et al., 2011), this value lies within the variability range over southern West Africa during the time period of the DACCIWA field campaign.

Importantly, MONC is not coupled to an interactive land surface scheme in the present study and so to represent the effects of the surface, time-varying fluxes of sensible and latent heat are prescribed using surface measurements from the Savé ground-site (Kohler et al., 2016). Fluxes from 5th July 2016 used to force the model are plotted in ~~Fig. ??~~figure 4b, for the simulation period indicated.

All the simulations presented in this paper use a domain size of 7.5 km x 7.5 km in the horizontal with a 30 m grid-spacing, and a vertical extent of 2 km with a 10 m spacing between vertical levels up to 1.5 km, increasing to a 20 m spacing between 1.5 km and 2 km. The top 500 m is a damping layer to prevent unwanted gravity waves from reflecting off the rigid model lid. The first ~~two hours~~ 90 minutes of each simulation (between 0330 - ~~0530~~ 0500 UTC) are discarded to allow ~~for model spin up~~the model to spin up from the initial conditions, and periodic boundary conditions are used in all cases.

3.2 Details of model experiments

Here we introduce and describe two initial experiments, the results from which are analysed in the next section.

The first MONC experiment ~~makes use of CASIM , and~~ with CASIM is configured for dual moment cloud and rain, while cold processes were not considered or required. Autoconversion and accretion are represented using the scheme of Khairoutdinov and Kogan (2000) and sedimentation of cloud droplets and rain is included. A saturation adjustment scheme is employed for condensation and evaporation of cloud droplets, while rain evaporation is based on the scheme used in the LEM (Gray et al., 2001). CASIM includes various options for aerosol activation and in the this work we ~~employed~~ employ the scheme of Abdul-Razzak et al. (1998), with the aerosol specified as a single accumulation mode log-normal size distribution following the analysis of regional aerosol properties in Haslett et al. (in preparation, 2018). The aerosol mass and number fields are completely passive in this experiment (i.e. not influenced by cloud and rain processes), and are used only to determine the number of droplets activated. This experiment is henceforth referred to as CASIM_NO_PROC.

The second MONC experiment ~~replaces CASIMwith the 'all or nothing' cloud scheme; we~~ is identical to CASIM_NO_PROC, the only difference being that droplet sedimentation is turned off following the 90 minute spin-up period to allow turbulence to develop within the boundary layer. We refer to this experiment as ~~SIMPLE_CLOUD. Since no precipitation was observed during the majority of the DACCIWA IOPs, including the present one, the~~ CASIM_NO_SED. The rationale of this second experiment is to explore whether a simulation with ~~such a basic representation of cloud~~ sedimentation disabled is able to reproduce the observations for this case, and therefore to reveal the extent to which ~~the additional complexity offered by CASIM~~ sedimentation impacts the simulation.

4 Results

We begin with an initial inspection of results from the CASIM_NO_PROC experiment. ~~Fig. ??~~ Figure 5a shows a time-height plot of the domain average cloud mass mixing ratio for the period ~~0530~~ 0500 UTC – 1100 UTC. The presence of a cloud layer

is revealed with an initial mean cloud base around 350 m, and a cloud top of 600 m. Following sunrise at 0537 UTC, the surface fluxes of sensible and latent heat increase sharply from around 0700 UTC as shown in ~~Fig ??~~figure 4b, resulting in a deeper boundary layer (BL) and lifting of the cloud layer from around 0800 UTC. The general trend in the timeseries of cloud base height is well captured by the model, as seen in the comparison against the ceilometer measurements from the Savé ground-site (~~fig ??~~figure 5b). Cloud top long wave radiative cooling was found to be crucial for the development and maintenance of the cloud, through the generation of an overturning circulation within the cloud layer. Indeed, without any long wave cooling, the model was unable to sustain the cloud layer, resulting in complete dissipation by the end of the spin-up period.

Figure 6 provides further information about the evolution of the mixing state of the simulated BL, in terms of profiles of liquid water potential temperature, liquid water mixing ratio and total water mixing ratio following the diagnostic analysis of Jones et al. (2011). Domain average profiles from 0530 UTC (~~fig~~figure 6a) reveal a predominantly well-mixed cloud-topped BL capped by a temperature inversion at 600m agl. A stable layer exists from the surface up to 150m agl, consistent with long wave cooling of the surface during the night, with a thin fog layer which dissipates by 0630 UTC. By 1100 UTC (~~fig~~figure 6b), the increase in surface fluxes produces a deeper, convective BL with an unstable layer at the surface. A well-mixed layer exists between 50m and 400m agl in the sub-cloud region, with a hint of a second shallower well-mixed layer directly below the top of the BL, where the values of liquid water mixing ratio are largest. These layers are separated by a transition region between 400m and 900m agl, where the liquid water potential temperature gradually increases with height. ~~The~~ Figure 7a and b shows that the model captures the general deepening of the BL as seen in the observations, with a simulated BL height of 1.1 km by 1100 UTC compared with 1 km in the corresponding radiosonde profile~~(Fig 2a,b)~~. The vertical structure of both potential temperature and relative humidity are also reasonably well captured by the model~~, as shown in (Fig 7a,b)~~.

~~Fig. ??~~ Figure 8a compares the timeseries of simulated LWP from CASIM_NO_PROC with observations from the vertically pointing ground-based microwave radiometer at Savé (Wieser et al., 2016). Because the radiometer measurements represent the time evolution at a single location, care must be taken when evaluating the model against this dataset to account for the difference in spatial sampling. Hence in ~~Fig. ??~~ figure 8 we plot both the simulated LWP timeseries taken from the centre of the model domain diagnosed at 1 minute intervals, together with the variability in LWP across the whole domain. The model simulates the evolution of LWP in a manner that is broadly consistent with the measurements, with the observations for the most part lying within +/- 2 standard deviations of the simulated LWP values. Peak local values of LWP also occur at approximately the correct time in the model as well, i.e. after 0800 UTC when the surface fluxes have started to rise sharply. No precipitation was produced by the model during the simulation period, consistent with the measurements at Savé.

Having validated the ability of CASIM_NO_PROC to capture the key features of the observations, we now consider the impact of ~~reducing the complexity of the cloud scheme~~ disabling sedimentation by analysing results from the ~~SIMPLE_CLOUD experiment. Fig ?? shows that SIMPLE_CLOUD~~ CASIM_NO_SED experiment. Figure 8b shows that CASIM_NO_SED underestimates the variability in LWP before 0730 UTC compared to both the observations and CASIM_NO_PROC. Maps comparing the spatial distribution of LWP within the model domain for both simulations (~~Fig.~~figure 9) confirm that the cloud is much more spatially homogeneous in ~~SIMPLE_CLOUD~~ CASIM_NO_SED initially, resembling a largely featureless sheet of stratus as opposed to the more lumpy stratocumulus seen in CASIM_NO_PROC. A comparison of the timeseries of mean

LWP in the domain (~~Fig~~solid lines in figure 10) reveals that, although both simulations show a similar rise and fall pattern with a peak around mid-morning, there are still some notable differences despite neither simulation producing any precipitation. For instance, following completion of the spin-up phase ~~, the values of LWP are very similar. But between 0530 - 0700~~ at 0500 UTC, the rate of LWP growth slows in ~~SIMPLE_CLOUD~~ CASIM_NO_SED relative to CASIM_NO_PROC such that by 0700 UTC, CASIM_NO_PROC has the higher LWP. The peak LWP in ~~SIMPLE_CLOUD~~ CASIM_NO_SED occurs around the same time but persists for longer, before decreasing sharply around 1000 UTC. The other difference between the two simulations is in the evolution of the domain mean cloud base height. ~~SIMPLE_CLOUD~~ Figure 5b shows that CASIM_NO_SED maintains an elevated cloud base height compared to CASIM_NO_PROC throughout the simulation period. Between 0530 - 0800 UTC, the mean cloud base height is 60 m higher in ~~SIMPLE_CLOUD~~CASIM_NO_SED, increasing to an average of 140 m higher between 0800 - 1100 UTC.

The ~~differences in the evolution of LWP and cloud base height between the two simulations can be explained through consideration of the effects of droplet sedimentation as a result of gravitational settling. There is no representation of either sedimentation or warm rain production in SIMPLE_CLOUD, whereas both processes are represented in CASIM_NO_PROC. However, values of rain water path in CASIM_NO_PROC are typically four orders of magnitude less than the liquid water path, and no precipitation reaches the surface, suggesting that droplet sedimentation and not the warm rain process is responsible for the differences between the simulations. This was confirmed by running a test simulation of CASIM_NO_PROC with droplet sedimentation switched off but autoconversion and accretion left switched on, which effectively yielded the same results as the SIMPLE_CLOUD simulation.~~

~~The~~ link between droplet sedimentation and LWP has been explored previously by Bretherton et al. (2007), in the context of nocturnal non-drizzling marine stratocumulus layers in the subtropics. Sedimentation was found to ultimately increase LWP, caused by the removal of liquid water from the entrainment zone near cloud top. In turn this reduces the magnitudes of evaporative cooling and long wave radiative cooling, two processes which control the sinking of relatively dry air from the free troposphere into the cloud layer. Conversely, higher CCN concentrations decrease the mean droplet size and fall speed, reducing sedimentation rates and thus making the cloud more susceptible to the effects of entrainment at the top of the BL. This results in a reduced LWP and a thinner cloud layer for more polluted conditions. We now conduct further analysis of the two MONC experiments to explore whether the results of the present study are consistent with the findings of Bretherton et al. (2007).

Returning to ~~Fig.~~figure 10, following completion of the spin-up phase at ~~0530~~ 0500 UTC, both simulations have ~~a very similar~~ the same value of LWP. As mentioned earlier, the initial development of the cloud layer during the spin-up phase is strongly dependent on the mechanism of long wave radiative cooling. ~~The~~ By 0530 UTC, the lack of droplet sedimentation in ~~SIMPLE_CLOUD does mean however~~ CASIM_NO_SED means that this experiment is able to maintain a slightly higher liquid water content at cloud top ~~during spin-up~~ relative to CASIM_NO_PROC, with a more sharply defined peak value (see ~~fig ?? compared to fig~~figure 6c compared to figure 6a). Over the following 1.5 hours~~up to 0700 UTC~~, the larger liquid water content ~~in SIMPLE_CLOUD~~ within the entrainment zone in CASIM_NO_SED promotes stronger evaporative cooling and long wave radiative cooling relative to CASIM_NO_PROC ~~, which~~ (see figure 11). This increases the downward heat flux at

cloud top, reduces moisture fluxes and reduces the circulation strength in the BL (~~fig~~figure 12). ~~This results in~~ The result is a slower rate of LWP growth with time relative to CASIM_NO_PROC, such that by ~~0700UTC~~0700 UTC, CASIM_NO_PROC has the higher LWP. Thus in CASIM_NO_PROC, the removal of liquid water mass from cloud top due to droplet sedimentation effectively acts to shield the cloud layer to some extent from the effects of entrainment, allowing LWP to grow faster with time.

A closer inspection of figure 11 reveals more information about the relative roles of radiative cooling and evaporative cooling in the evolution of the cloud layer. In both simulations, it is clear that radiative cooling is the dominant process, with peak rates that are typically an order of magnitude larger than those produced by evaporation near cloud top. The absence of sedimentation in CASIM_NO_SED results in larger cooling rates associated with both processes. However, the increase in longwave cooling rates is relatively modest - around 37% by 0700 UTC - whereas evaporative cooling rates increase by a factor of 2 within the same time period. Thus in relative terms, the effect of sedimentation appears to have the largest impact on rates of evaporative cooling.

It is important to remember that the present study is over land and the simulation period extends into the day time, as opposed to the nocturnal marine BL simulated by Bretherton et al. (2007). Thus it is no surprise that after 0800 UTC, when the fluxes of sensible and latent heat dominate and the surface layer becomes unstable, the effect of sedimentation on LWP starts to break down. The convective vertical mixing associated with the prescribed sensible and latent heat fluxes coincide with the lifting of the cloud layer and a decrease in LWP, with a more rapid depletion evident in CASIM_NO_PROC (figure 10). This is consistent with stronger evaporative cooling during mixing associated with the higher LWP around 0730 UTC.

It is interesting to consider what would happen to the evolution of LWP in the absence of surface driven mixing. This is important because, although the mean LLC onset time at Savé is 0300 UTC (around three hours before sunrise), it is notably earlier at other ground-sites (e.g. 0000 UTC in Kumasi, and 2100 UTC at Ile-Ife; Kalthoff et al. 2017). Assuming the sedimentation-entrainment feedback holds true, an earlier LLC onset would allow more time for the effects of sedimentation to impact LWP before sunrise. To explore this idea, both experiments were re-run with surface fluxes set to zero throughout and with short wave radiation turned off for the duration of the simulation. The forcing of the low-level jet was left unchanged. The results are shown as dashed lines in figure ~~??~~10. As anticipated, it can clearly be seen that when nocturnal conditions are maintained, CASIM_NO_PROC ~~maintains~~ exhibits a higher LWP by around 33% relative to ~~SIMPLE_CLOUD~~ CASIM_NO_SED by the end of the simulation period. Based on this analysis, we conclude that the response of the model is consistent with the reasoning of Bretherton et al. (2007).

5 Discussion

The numerical experiments performed in this study have shown that droplet sedimentation helps to promote a more heterogeneous cloud layer, with localised regions of both enhanced LWP and reduced LWP within the model domain relative to simulations without droplet sedimentation, whilst also lowering cloud base height. Whilst surface fluxes remain relatively small, in this case prior to 0700 UTC, sedimentation also acts to increase the rate of mean LWP growth within the domain,

by buffering the cloud layer from the effects of ~~entrainment-induced evaporative cooling~~ cloud top entrainment driven by evaporative cooling and long wave radiative cooling.

Since droplet sedimentation rates are inversely proportional to number concentration, one would expect the effects of sedimentation on both LWP and cloud base height to become more prominent as cloud droplet number concentration (CDNC) reduces. In the case of CASIM_NO_PROC, predicted number concentrations lie in the range 400-700 cm^{-3} at STP, which agrees well with in-situ measurements with median values of around 500 cm^{-3} at STP (J. Taylor, personal communication, 2018). In this section we perform some new experiments to explore the sensitivity to reducing CDNC. We introduce results from a new experiment, CASIM_200, which prescribes the initial CDNC to be 200 cm^{-3}. This new simulation produces excessive variability in the LWP field and cloud bases that are too low (~~figs~~figures 13 and 14 respectively), confirming our hypothesis. This was found to be the case even with autoconversion switched off. The depth of the BL in CASIM_200 is also too shallow by the end of the simulation period, by virtue of the effect of increased droplet size and excessive sedimentation velocity on entrainment. However, mean LWP is slightly lower compared to CASIM_NO_PROC; this is because, around 0830 UTC, cloud base becomes so low it touches the surface and liquid water is removed from the domain. At 200 cm^{-3}, this removal of liquid is predominantly due to gravitational settling of cloud droplets as opposed to significant warm rain production. Further reductions in CDNC, down to 100/cc and 50/cc respectively, deplete the LWP even more as a result of an increase in autoconversion. These results, as summarised in table 1, suggest that the effects of droplet size on cloud-top entrainment rates should not be ignored when considering the diurnal cycle of LLCs in the region.

In light of this result, it is pertinent to consider the potential implications of changes in CDNC in terms of cloud radiative effects. Any elevation of CDNC within urban plumes will increase cloud optical depth in a manner that is proportional to $CDNC^{1/3}$ and $LWP^{2/3}$ for shallow clouds. However, the reduced sedimentation associated with the increased CDNC would increase cloud-top entrainment and therefore reduce LWP. Hence any effect of increased optical thickness arising from enhanced aerosol concentrations will to some extent be offset by the sedimentation-entrainment feedback, and is likely to lessen any first order indirect effect.

Our findings also have implications for the diagnosis of aerosol-cloud interactions from satellite data. An adiabatic cloud profile is typically assumed when estimating cloud properties from satellites, but a relevant issue here is the extent to which the adiabatic assumption holds in these low level clouds (Merk et al., 2016). Since satellites view cloud top, it is conceivable that the sedimentation-entrainment effect may well bias retrievals significantly.

An important caveat in our results is the prescription of surface fluxes in our simulations; there is no feedback between changes in cloud cover, LWP and the land surface radiation budget. What happens after sunrise in reality is likely to be dependent on such feedbacks, which the present model configuration is not able to capture due to the lack of an interactive land surface scheme. Coupling of MONC to an interactive land surface scheme is needed to be able to comment fully on the impacts of droplet sedimentation and cloud optical depth on the diurnal cycle of these low level clouds.

6 Conclusions

In this study, large eddy simulations of low level clouds over southern West Africa have been performed with a focus on establishing the sensitivity of the cloud evolution to ~~different treatments of the microphysics~~the treatment of droplet sedimentation. The simulations are constrained and validated using the unprecedented suite of measurements collected during the DACCIWA field campaign in 2016.

Our results reveal that, even for non-precipitating clouds, the evolution of low level clouds over southern West Africa is sensitive to the effects of droplet sedimentation, suggesting that this mechanism should not be neglected when performing large scale simulations of the region. Sedimentation of droplets acts to remove liquid water from the entrainment zone near cloud top, reducing the magnitude of evaporative cooling and longwave radiative cooling during entrainment mixing. This increases the rate of growth of liquid water path during the night time and early morning period. For the conditions of prescribed subsidence and surface fluxes, the simulation best able to reproduce the observations was the one that came closest to matching the observed droplet number concentrations. Ignoring droplet sedimentation completely reduced variability in liquid water path by around a factor of 2 during the early morning, and also elevated the mean cloud base height by an additional 200 m by the end of the simulation period. Conversely, overestimating sedimentation rates, by virtue of reducing the droplet number concentration by a factor of two or more relative to observed values, caused cloud base to lower to the surface by 0830 UTC, and liquid water path variability to increase around a factor of 2. Both these changes degraded the realism of the model simulation with respect to the available observations. In all cases, cloud top long wave radiative cooling during the night was found to be crucial for the formation and maintenance of the clouds.

The link between sedimentation and liquid water path has been noted previously in relation to nocturnal non-drizzling marine boundary layer clouds. But the clouds considered in the present study form over land and persist into the day time, which means that the effect of sedimentation can potentially play an important role in regulating the surface radiation budget, with consequences for the diurnal cycle of the boundary layer in southern West Africa and possibly the circulation of the West African Monsoon. The results of our study suggest the possibility of a complex feedback chain involving aerosols, sedimentation, entrainment, liquid water path and surface energy fluxes. We recommend as part of future work that the experiments performed ~~as part of~~ in this study be repeated using an interactive land surface scheme, to determine the extent to which the sensitivities shown are modified due to feedbacks between cloud cover and the surface heat flux budget.

Code and data availability. The observational data used in this paper can be accessed upon request at http://baobab.sedoo.fr/DACCIWA. The MONC, CASIM and SOCRATES codes are maintained by the Met Office and accessible via the Met Office Science Repository Service (https://code.metoffice.gov.uk/):

MONC branch: main/branches/dev/chrisdearden/r4366_dacciwa_socrates_vn0.8_vn0.9_part2

CASIM branch: casim/branches/dev/chrisdearden/r4323_casim_vn10.8_monc_fixes

For further details, please contact Christopher Dearden (c.dearden@leeds.ac.uk) or Adrian Hill (adrian.hill@metoffice.gov.uk).

Competing interests. The authors declare that they have no conflict of interest.

Acknowledgements. The research leading to these results has received funding from the European Union 7th Framework Programme (FP7/2007-2013) under Grant Agreement no. 603502 (EU project DACCIWA: Dynamics-aerosol-chemistry-cloud interactions in West Africa).The authors would like to acknowledge Norbert Kalthoff, Bianca Adler, Karmen Babic, Fabienne Lohou, Cheikh Dione, Marie Lothon and Xabier Pedruzo Bagazgoitia for their role in producing the observations presented in this paper, and for helpful discussions at the DACCIWA project meeting in Karlsruhe, Germany, 24-27 October 2017. This work used the ARCHER UK National Supercomputing Service (http://www.archer.ac.uk) and the JASMIN service (http://www.jasmin.ac.uk).

References

Abdou, K., Parker, D. J., Brooks, B., Kalthoff, N., and Lebel, T.: The diurnal cycle of lower boundary-layer wind in the West African monsoon, Quart. J. Roy. Met. Soc., 136, 66–76, https://doi.org/10.1002/qj.536, 2010.

Abdul-Razzak, H., Ghan, S. J., and Rivera-Carpio, C.: A parameterization of aerosol activation - 1. Single aerosol type, J. Geophys. Res-Atmos., 103, 6123–6131, 1998.

Ackerman, A., Kirkpatrick, M. P., Stevens, D. E., and Toon, O. B.: The impact of humidity above stratiform clouds on indirect aerosol climate forcing, Nature, 432, 1014–1017, https://doi.org/10.1038/nature03174, 2004.

Adler, B., Kalthoff, N., and Gantner, L.: Nocturnal low-level clouds over southern West Africa analysed using high-resolution simulations, Atmos. Chem. Phys., 17, 899–910, https://doi.org/10.5194/acp-17-899-2017, 2017.

Bain, C. L., Parker, D. J., Taylor, C. M., Kergoat, L., and Guichard, F.: Observations of the Nocturnal Boundary Layer Associated with the West African Monsoon, Mon. Wea. Rev., 138, 3142–3156, https://doi.org/10.1175/2010MWR3287.1, 2010.

Birch, C. E., Parker, D. J., Marsham, J. H., Copsey, D., and Garcia-Carreras, L.: A seamless assessment of the role of convection in the water cycle of the West African Monsoon, J. Geophys Res-Atmos, 119, 2890–2912, https://doi.org/10.1002/2013JD020887, 2014.

Bretherton, C. S., Blossey, P. N., and Uchida, J.: Cloud droplet sedimentation, entrainment efficiency, and subtropical stratocumulus albedo, Geophys. Res. Lett., 34, https://doi.org/10.1029/2006GL027648, 2007.

Brown, A.: The sensitivity of large-eddy simulations of shallow cumulus convection to resolution and subgrid model, Quart. J. Roy. Meteor. Soc., 125, 469–482, https://doi.org/10.1002/qj.49712555405, 1999.

Brown, A. R., Cederwall, R., Chlond, A .and Duynkerke, P. G., Golaz, J., Khairoutdinov, M., Lewellen, D. C., Lock, A. P., MacVean, M. K., Moeng, C. H., Neggers, R. A. J., Siebesma, A. P., and Stevens, B.: Large-eddy simulation of the diurnal cycle of shallow cumulus convection overland, Quart. J. Roy. Met. Soc., 128, 1075–1093, https://doi.org/10.1256/003590002320373210, 2002.

Brown, N., Weiland, M., Hill, A., Shipway, B., Maynard, C., Allen, T., and Rezny, M.: A Highly Scalable Met Office NERC Cloud Model, in: Proceedings of the 3rd International Conference on Exascale Applications and Software, pp. 132–137, University of Edinburgh, Edinburgh, Scotland, UK, http://dl.acm.org/citation.cfm?id=2820083.2820108, 2015.

Clark, P. D., Choularton, T. W., Brown, P. R. A., Field, P. R., Illingworth, A. J., and Hogan, R. J.: Numerical modelling of mixed-phase frontal clouds observed during the CWVC project, Quart. J. Roy. Met. Soc., 131, 1677–1693, https://doi.org/10.1256/qj.03.210, 2005.

Connolly, P. J., Choularton, T. W., Gallagher, M. W., Bower, K. N., Flynn, M. J., and Whiteway, J. A.: Cloud-resolving simulations of intense tropical Hector thunderstorms: Implications for aerosol-cloud interactions, Quart. J. Roy. Met. Soc., 132, 3079–3106, https://doi.org/10.1256/qj.05.86, 2006.

Connolly, P. J., Vaughan, G., Cook, P., Allen, G., Coe, H., Choularton, T. W., Dearden, C., and Hill, A.: Modelling the effects of gravity waves on stratocumulus clouds observed during VOCALS-UK, Atmos. Chem. Phys., 13, 7133–7152, https://doi.org/10.5194/acp-13-7133-2013, 2013.

Dee, D. P., Uppala, S. M., Simmons, A. J., Berrisford, P., Poli, P., Kobayashi, S., Andrae, U., Balmaseda, M. A., Balsamo, G., Bauer, P., Bechtold, P., Beljaars, A. C. M., van de Berg, L., Bidlot, J., Bormann, N., Delsol, C., Dragani, R., Fuentes, M., Geer, A. J., Haimberger, L., Healy, S. B., Hersbach, H., Hólm, E. V., Isaksen, L., Kållberg, P., Köhler, M., Matricardi, M., McNally, A. P., Monge-Sanz, B. M., Morcrette, J.-J., Park, B.-K., Peubey, C., de Rosnay, P., Tavolato, C., Thépaut, J.-N., and Vitart, F.: The ERA-Interim reanalysis: configuration and performance of the data assimilation system, Quarterly Journal of the Royal Meteorological Society, 137, 553–597, https://doi.org/10.1002/qj.828, http://dx.doi.org/10.1002/qj.828, 2011.

Derrien, S., Bezombes, Y., Bret, G., Gabella, O., Jarnot, C., Medina, P., Piques, E., Delon, C., Dione, C., Campistron, B., Durand, P., Jambert, C., Lohou, F., Lothon, M., Pacifico, F., and Meyerfeld, Y.: DACCIWA field campaign, Savè super-site, UPS instrumentation; SEDOO OMP., http://dx.doi.org/10.6096/DACCIWA.1618, 2016.

Dione, C., Lohou, F., Lothon, M., Adler, B., Babic, K., Kalthoff, N., Pedruzo-Bagazgoitia, X., Bezombes, Y., and Gabella, O.: Intra-seasonal evolution of the most important low-troposphere dynamical structures over southern West Africa during DACCIWA field campaign, Prepared for submission to Atmos. Chem. Phys.,, 2018.

Edwards, J. M. and Slingo, A.: Studies with a flexible new radiation code. I: Choosing a configuration for a large-scale model, Quart. J. Roy. Met. Soc., 122, 689–719, https://doi.org/10.1002/qj.49712253107, http://dx.doi.org/10.1002/qj.49712253107, 1996.

Flamant, C., Knippertz, P., Fink, A., Akpo, A., Brooks, B., Chiu, C., Coe, H., Danuor, S., Evans, M., Jegede, O., Kalthoff, N., Konaré, A., Liousse, C., Lohou, F., Mari, C., Schlager, H., Schwarzenboeck, A., Adler, B., Amekudzi, L., Aeyee, J., Ayoola, M., Bessardon, G., Bower, K., Burnet, F., Catoire, V., Colomb, A., Fossu-Amankwah, K., Lee, J., Lothon, M., Manaran, M., Marsham, J., Meynadier, R., Ngamini, J.-B., Rosenberg, P., Sauer, D., Schneider, J., Smith, V., Stratmann, G., Voigt, C., and Yoboue, V.: The Dynamics-Aerosol-Chemistry-Cloud Interactions in West Africa field campaigns: Overview and research highlights, Bull. Amer. Meteor. Soc., https://doi.org/10.1175/BAMS-D-16-0256.1, 2017.

Garcia-Carreras, L., Marsham, J. H., Parker, D. J., Bain, C. L., Milton, S., Saci, A., Salah-Ferroudj, M., Ouchene, B., and Washington, R.: The impact of convective cold pool outflows on model biases in the Sahara, Geophys. Res. Lett., 40, 1647–1652, https://doi.org/10.1002/grl.50239, 2013.

Gounou, A., Guichard, F., and Couvreux, F.: Observations of Diurnal Cycles Over a West African Meridional Transect: Pre-Monsoon and Full-Monsoon Seasons, Boundary-layer Meteorology, 144, 329–357, https://doi.org/10.1007/s10546-012-9723-8, 2012.

Gray, M. E. B., Petch, J., Derbyshire, S. H., Brown, A. R., Lock, A. P., Swann, H. A., and Brown, P. R. A.: Version 2.3 of the Met Office large eddy model: Part II Scientific Documentation, Apr turbulence and diffusion report 276, Met Office, Fitroy Road, Exeter EX1 3PB, United Kingdom, 2001.

Grosvenor, D. P., Field, P. R., Hill, A. A., and Shipway, B. J.: The relative importance of macrophysical and cloud albedo changes for aerosol-induced radiative effects in closed-cell stratocumulus: insight from the modelling of a case study, Atmos. Chem. Phys., 17, 5155–5183, https://doi.org/10.5194/acp-17-5155-2017, https://www.atmos-chem-phys.net/17/5155/2017/, 2017.

Handwerker, J., Scheer, S., and Gamer, T.: DACCIWA field campaign, Savè super-site, Cloud and precipitation; SEDOO OMP., http://dx.doi.org/10.6096/DACCIWA.1686, 2016.

Hannak, L., Knippertz, P., Fink, A. H., A. Kniffka, A., and Pante, G.: Why Do Global Climate Models Struggle to Represent Low-Level Clouds in the West African Summer Monsoon?, J. Clim., 30, 1665–1687, https://doi.org/10.1175/JCLI-D-16-0451.1, 2017.

Haslett, S., Coe, H., and Taylor, J.: Biomass burning from central Africa dominates regional pollution across the West African region during the monsoon season, in preparation, 2018.

Jones, C. R., Bretherton, C. S., and Leon, D.: Coupled vs. decoupled boundary layers in VOCALS-REx, Atmos. Chem. Phys., 11, 7143–7153, https://doi.org/10.5194/acp-11-7143-2011, 2011.

Kalthoff, N., Lohou, F., Brooks, B., Jegede, G., Adler, B., Babić, K., Dione, C., Ajao, A., Amekudzi, L. K., Aryee, J. N. A., Ayoola, M., Bessardon, G., S, K. D., Handwerker, J., Kohler, M., Lothon, M., Pedruzo-Bagazgoitia, X., Smith, V., Sunmonu, L., A.Wieser, Fink, A. H., and Knippertz, P.: An overview of the diurnal cycle of the atmospheric boundary layer during the West African monsoon season: Results from the 2016 observational campaign, Atmos. Chem. Phys. Discuss., 2017, 1–23, https://doi.org/10.5194/acp-2017-631, https://www.atmos-chem-phys-discuss.net/acp-2017-631/, 2017.

Khairoutdinov, M. and Kogan, Y.: A new cloud physics parameterization in a large-eddy simulation model of marine stratocumulus, Mon. Wea. Rev., 128, 229–243, https://doi.org/10.1175/1520-0493(2000)128<0229:ANCPPI>2.0.CO;2, 2000.

Knippertz, P., Fink, A. H., Schuster, R., Trentmann, J., Schrage, J. M., and Yorke, C.: Ultra-low clouds over the southern West African monsoon region, Geophys. Res. Lett., 38, https://doi.org/10.1029/2011GL049278, 2011.

Knippertz, P., Coe, H., Chiu, J. C., Evans, M. J., Fink, A. H., Kalthoff, N., Liousse, C., Mari, C., Allan, R. P., Brooks, B., Danour, S., Flamant, C., Jegede, O. O., Lohou, F., and Marsham, J. H.: The DACCIWA Project Dynamics-Aerosol-Chemistry-Cloud Interactions in West Africa, Bull. Amer. Met. Soc., 96, 1451–1460, https://doi.org/10.1175/BAMS-D-14-00108.1, 2015a.

Knippertz, P., Evans, M. J., Field, P. R., Fink, A. H., Liousse, C., and Marsham, J. H.: The possible role of local air pollution in climate change in West Africa, Nature Climate Change, 5, 815–822, https://doi.org/10.1038/NCLIMATE2727, 2015b.

Knippertz, P., Fink, A. H., Deroubaix, A., Morris, E., Tocquer, F., Evans, M. J., Flamant, C., Gaetani, M., Lavaysse, C., Mari, C., Marsham, J. H., Meynadier, R., Affo-Dogo, A., Bahaga, T., Brosse, F., Deetz, K., Guebsi, R., Latifou, I., Maranan, M., Rosenberg, P. D., and Schlueter, A.: A meteorological and chemical overview of the DACCIWA field campaign in West Africa in June-July 2016, Atmos. Chem. Phys., 17, 10 893–10 918, https://doi.org/10.5194/acp-17-10893-2017, 2017.

Kohler, M., Kalthoff, N., Seringer, J., and Kraut, S.: DACCIWA field campaign, Savè super-site, Surface measurements; SEDOO OMP, http://dx.doi.org/10.6096/DACCIWA.1690, 2016.

LeBarbé, L., Lebel, T., and Tapsoba, D.: Rainfall variability in West Africa during the years 1950-90, J. Clim., 15, 187–202, https://doi.org/10.1175/1520-0442(2002)015<0187:RVIWAD>2.0.CO;2 , 2002.

Lothon, M., Said, F., Lohou, F., and Campistron, B.: Observation of the diurnal cycle in the low troposphere of West Africa, Mon. Wea. Rev, 136, 3477–3500, https://doi.org/10.1175/2008MWR2427.1, 2008.

Marsham, J., Dixon, N. S., Garcia-Carreras, L., Lister, G. M. S., Parker, D. J., and Birch, P. K. C. E.: The role of moist convection in the West African monsoon system: Insights from continental-scale convection-permitting simulations, Geophys. Res. Lett., 40, 1843–1849, https://doi.org/10.1002/grl.50347, 2013.

Marsham, J. H., Dobbie, S., and Hogan, R. J.: Evaluation of a large-eddy model simulation of a mixed-phase altocumulus cloud using microwave radiometer, lidar and Doppler radar data, Quart. J. Roy. Met. Soc., 132, 1693–1715, https://doi.org/10.1256/qj.05.145, 2006.

Merk, D., Deneke, H., Pospichal, B., and Seifert, P.: Investigation of the adiabatic assumption for estimating cloud micro- and macrophysical properties from satellite and ground observations, Atmos. Chem. Phys., 16, 933–952, https://doi.org/10.5194/acp-16-933-2016, 2016.

Miltenberger, A. K., Field, P. R., Hill, A. A., Rosenberg, P., Shipway, B. J., Wilkinson, J. M., Scovell, R., and Blyth, A. M.: Aerosol-cloud interactions in mixed-phase convective clouds. Part 1: Aerosol perturbations, Atmos. Chem. Phys. Discuss., 2017, 1–45, https://doi.org/10.5194/acp-2017-788, https://www.atmos-chem-phys-discuss.net/acp-2017-788/, 2017.

Parker, D. J., Burton, R. R., Diongue-Niang, A., Ellis, R. J., Felton, M., Taylor, C. M., Thorncroft, C. D., Bessemoulin, P., and Tompkins, A. M.: The diurnal cycle of the West African monsoon circulation, Quart. J. Roy. Met. Soc., 131, 2839–2860, https://doi.org/10.1256/qj.04.52, 2005.

Schrage, J. M. and Fink, A. H.: Nocturnal Continental Low-Level Stratus over Tropical West Africa: Observations and Possible Mechanisms Controlling Its Onset, Mon. Wea. Rev., 140, 1794–1809, https://doi.org/10.1175/MWR-D-11-00172.1, 2012.

Schuster, R., P., A. H. F., and Knippertz: Formation and Maintenance of Nocturnal Low-Level Stratus over the Southern West African Monsoon Region during AMMA 2006, J. Atmos. Sci., 70, 2337–2355, https://doi.org/10.1175/JAS-D-12-0241.1, 2013.

Stevens, R. G., Loewe, K., Dearden, C., Dimitrelos, A., Possner, A., Eirund, G. K., Raatikainen, T., Hill, A. A., Shipway, B. J., Wilkinson, J., Romakkaniemi, S., Tonttila, J., Laaksonen, A., Korhonen, H., Connolly, P., Lohmann, U., Hoose, C., Ekman, A. M. L., Carslaw, K. S., and

Field, P. R.: A Model Intercomparison of CCN-Limited Tenuous Clouds in the High Arctic, Atmos. Chem. Phys. Discuss., 2017, 1–42, https://doi.org/10.5194/acp-2017-1128, https://www.atmos-chem-phys-discuss.net/acp-2017-1128/, 2017.

Sultan, B. and Janicot, S.: Abrupt shift of the ITCZ over West Africa and intra-seasonal variability, Geophys. Res. Lett., 27, 3353–3356, https://doi.org/10.1029/1999GL011285, 2000.

van der Linden, R., Fink, A. H., and Redl, R.: Satellite-based climatology of low-level continental clouds in southern West Africa during the summer monsoon season, J. Geophys Res-Atmos, 120, 1186–1201, https://doi.org/10.1002/2014JD022614, 2015.

Walters, D., Boutle, I., Brooks, M., Melvin, T., Stratton, R., Vosper, S., Wells, H., Williams, K., Wood, N., Allen, T., Bushell, A., Copsey, D., Earnshaw, P., Edwards, J., Gross, M., Hardiman, S., Harris, C., Heming, J., Klingaman, N., Levine, R., Manners, J., Martin, G., Milton, S., Mittermaier, M., Morcrette, C., Riddick, T., Roberts, M., Sanchez, C., Selwood, P., Stirling, A., Smith, C., Suri, D., Tennant, W., Vidale, P. L., Wilkinson, J., Willett, M., Woolnough, S., and Xavier, P.: The Met Office Unified Model Global Atmosphere 6.0/6.1 and JULES Global Land 6.0/6.1 configurations, Geosci. Mod. Devel., 10, 1487–1520, https://doi.org/10.5194/gmd-10-1487-2017, https://www.geosci-model-dev.net/10/1487/2017/, 2017.

Wieser, A., Adler, B., and Deny, B.: DACCIWA field campaign, Savè super-site, Thermodynamic data sets; SEDOO OMP., http://dx.doi.org/10.6096/DACCIWA.1659, 2016.

Young, G., Connolly, P. J., Jones, H. M., and Choularton, T. W.: Microphysical sensitivity of coupled springtime Arctic stratocumulus to modelled primary ice over the ice pack, marginal ice, and ocean, Atmos. Chem. Phys., 17, 4209–4227, https://doi.org/10.5194/acp-17-4209-2017, 2017.

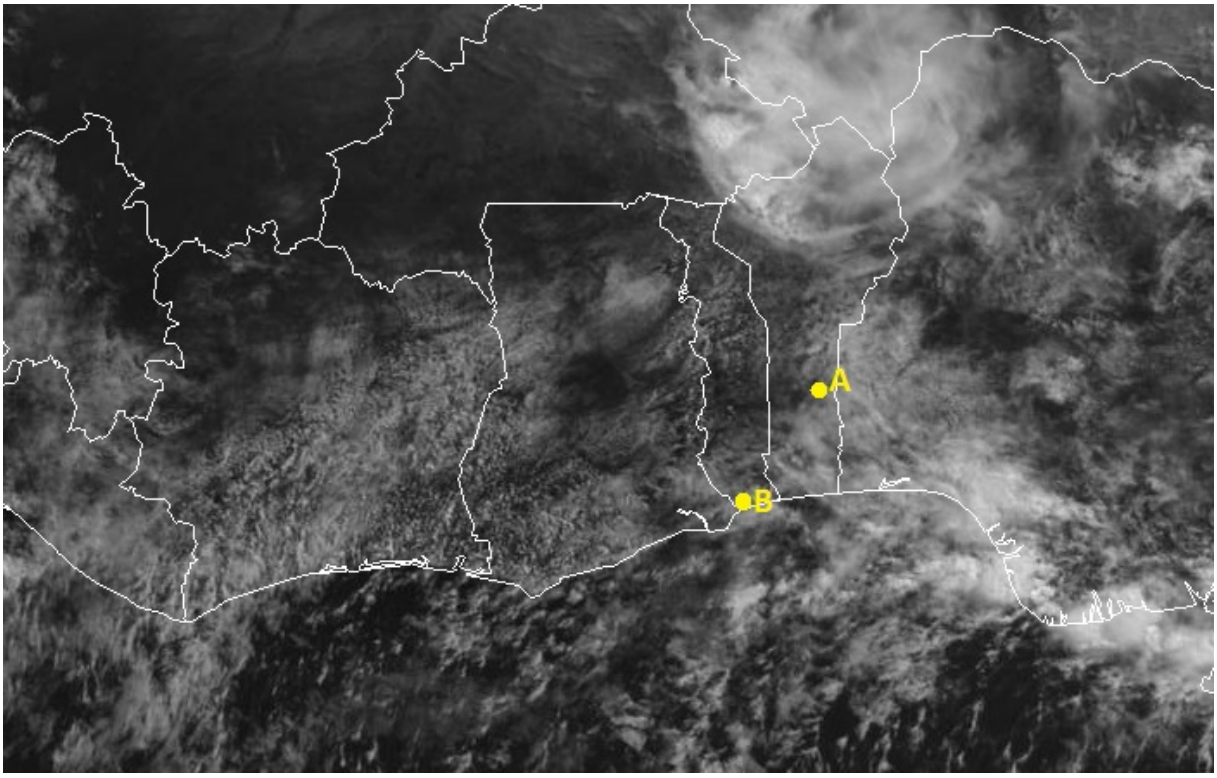

Figure 1. Image from the 0.6 μ Visible channel of the Meteosat-10 geostationary satellite, revealing the cloud structure over southern West Africa at 1012 UTC on 5 July 2016. Borders and coastlines are highlighted, along with the locations of Savé and Lome, labelled 'A' and 'B' respectively. Image obtained from http://catalogue.ceda.ac.uk/uuid/5fa2529b973e47ae38ab3557f2018ef4 (link valid as of July 2018).

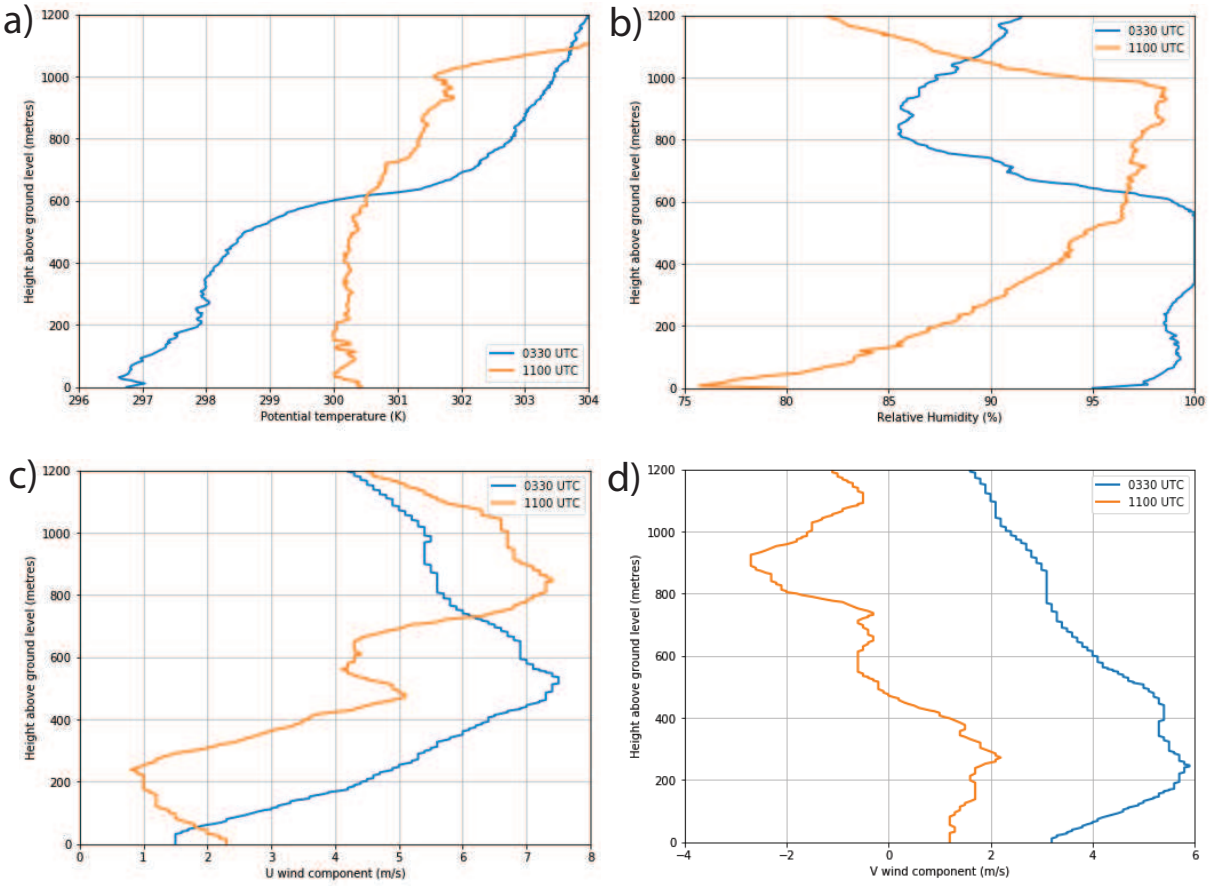

Figure 2. Profiles of a) potential temperature, b) relative humidity, c) u wind component and d) v wind component from radiosondes launched at Savé on 5 July 2016 at 0330 UTC (blue) and 1100 UTC (orange).

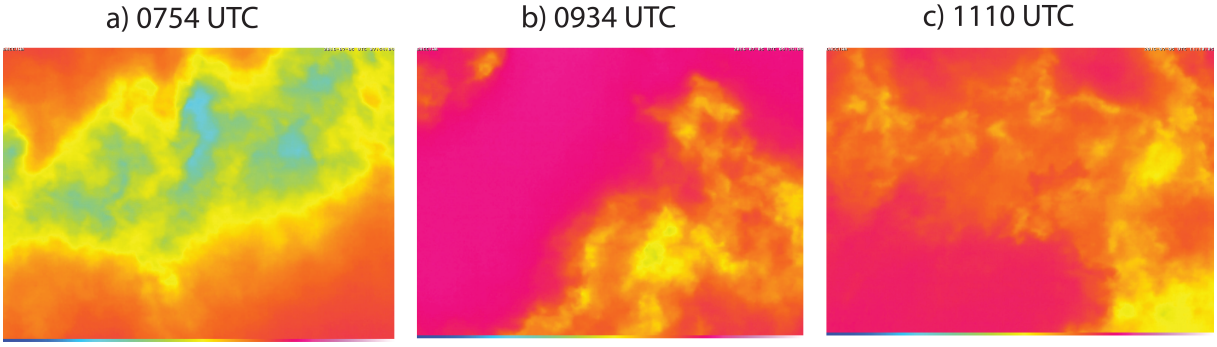

Figure 3. Images from the Infrared cloud camera at Savé on 5 July 2016 ~~(Handwerker et al., 2016)~~ (Derrien et al., 2016) for the times indicated. The images from the camera are coded in RGB colors (red, green, and blue), providing a qualitative estimate of cloud cover during the day and night. The image colour is dependent on the emissivity of the sky and consequently on the brightness temperature, such that red indicates warm and blue cold.

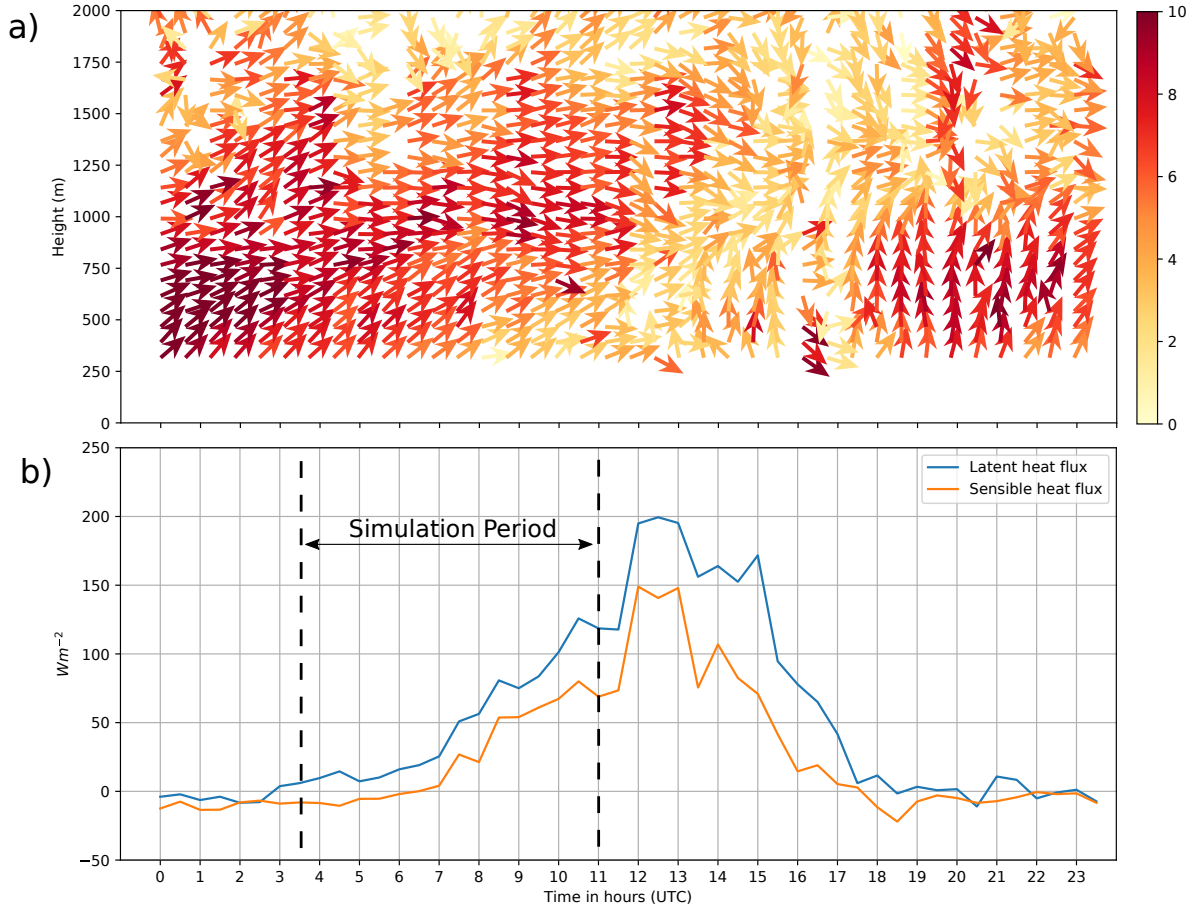

Figure 4. a) Time-height plot showing the vertical profile of the horizontal wind at Savé on 5 July 2016, from the Ultra-High Frequency wind profiler (Derrien et al., 2016). Wind vectors are normalised and indicate the direction of the horizontal flow; shading indicates the wind speed (m s^{-1}). b) Timeseries of latent heat flux (blue) and sensible heat flux (orange) from the Savé ground-site on 5 July 2016 (Kohler et al. 2016).

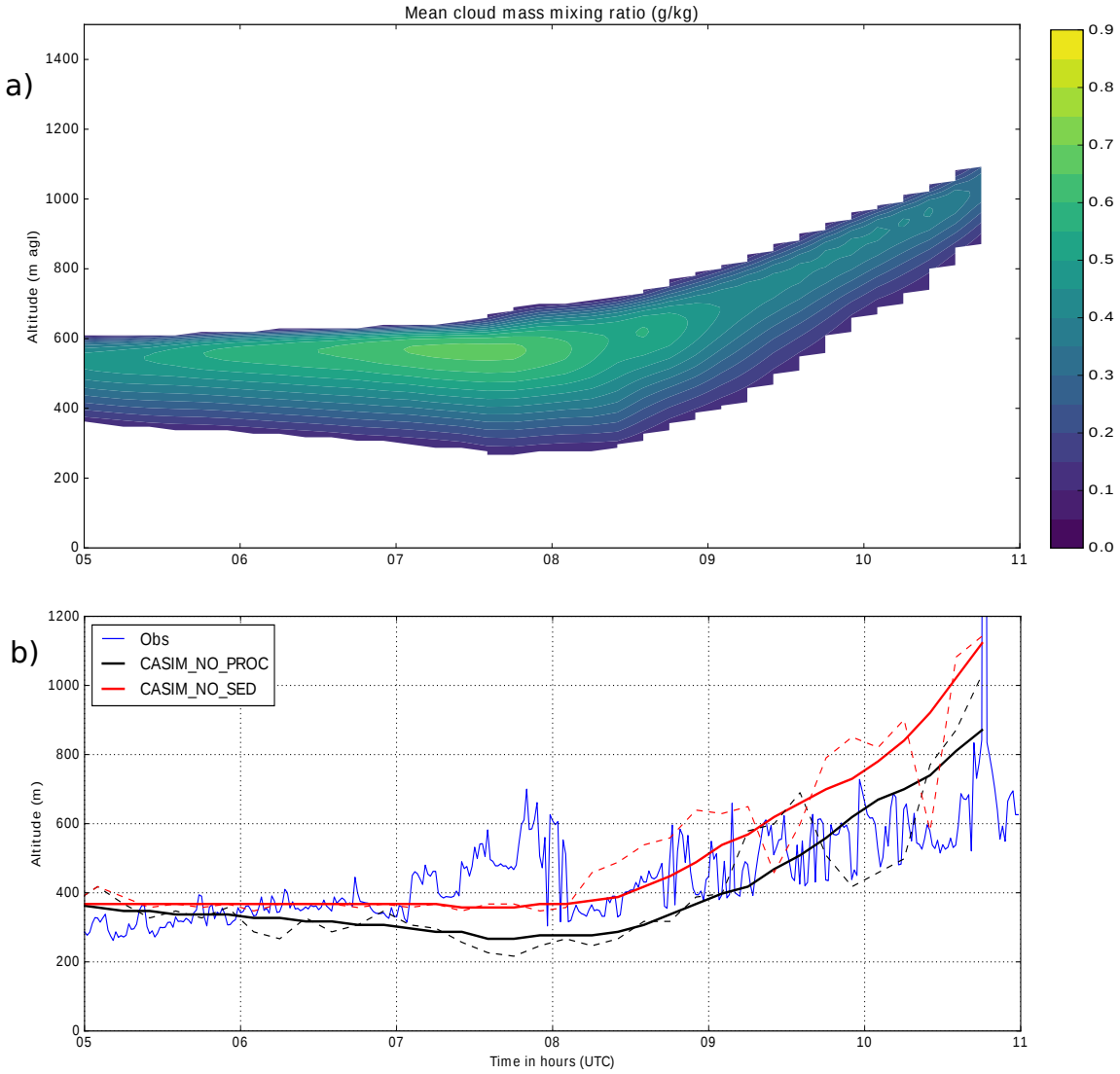

Figure 5. a) Time-height plot of the mean cloud mass mixing ratio (g kg^{-1}) within the model domain from the CASIM_NO_PROC experiment. Values are calculated as temporal means every 10 minutes. b) Timeseries of cloud base height at Savé on 5 July 2016 (blue) derived from ceilometer measurements (Handwerker et al. 2016), and 10 minute averages of cloud base height diagnosed from CASIM_NO_PROC and CASIM_NO_SED using a threshold cloud liquid water mass mixing ratio of 0.1 g kg^{-1}. Solid black/red line - domain mean value; dashed black/red line - the value at the centre of the model domain.

~~Vertical profiles of liquid water potential temperature (K; black lines), total water mass mixing ratio (g kg^{-1}; blue lines) and liquid water mass mixing ratio (x 10 g kg^{-1}; green lines) diagnosed at a) 0530 UTC and b) 1100 UTC from the CASIM_NO_PROC experiment.~~

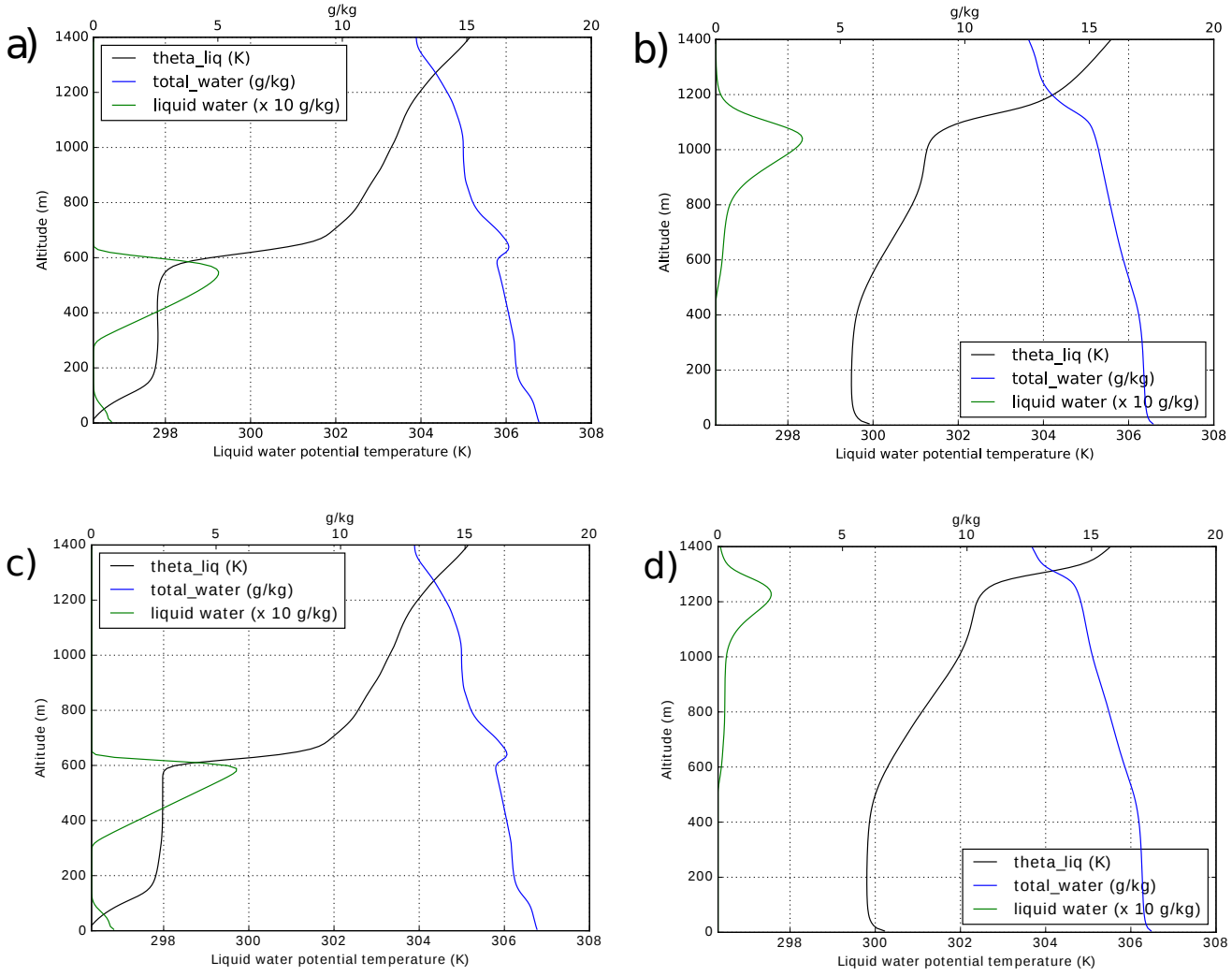

Figure 6. Vertical profiles of liquid water potential temperature (K; black lines), total water mass mixing ratio (g kg^{-1}; blue lines) and liquid water mass mixing ratio (x 10 g kg^{-1}; green lines) diagnosed at a) 0530 UTC and b) 1100 UTC from the CASIM_NO_PROC experiment. Equivalent plots for CASIM_NO_SED are shown in c) and d) respectively.

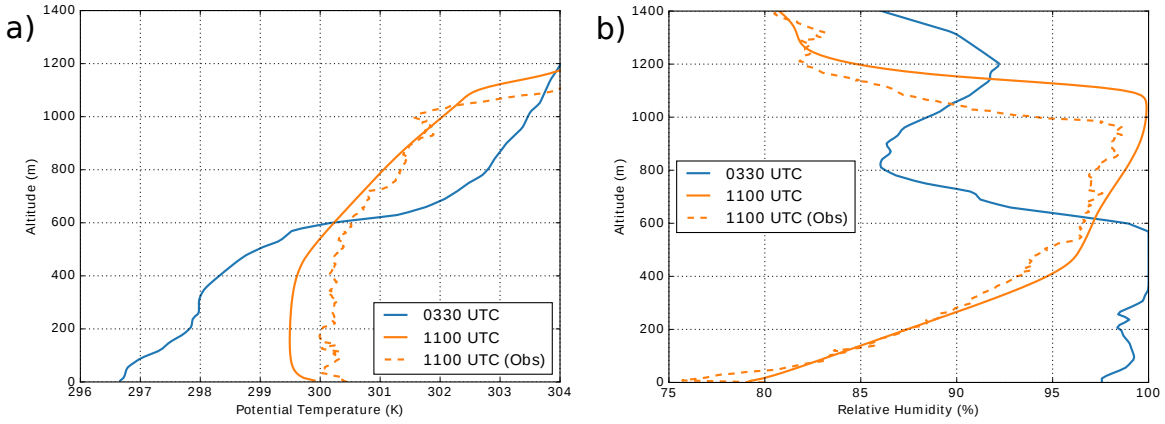

Figure 7. Simulated domain-average vertical profiles of a) potential temperature and b) relative humidity from the CASIM_NO_PROC simulation, calculated at 0330 UTC (blue) and 1100 UTC (orange). In each case the dashed orange line corresponds to the radiosonde profile from 1100 UTC.

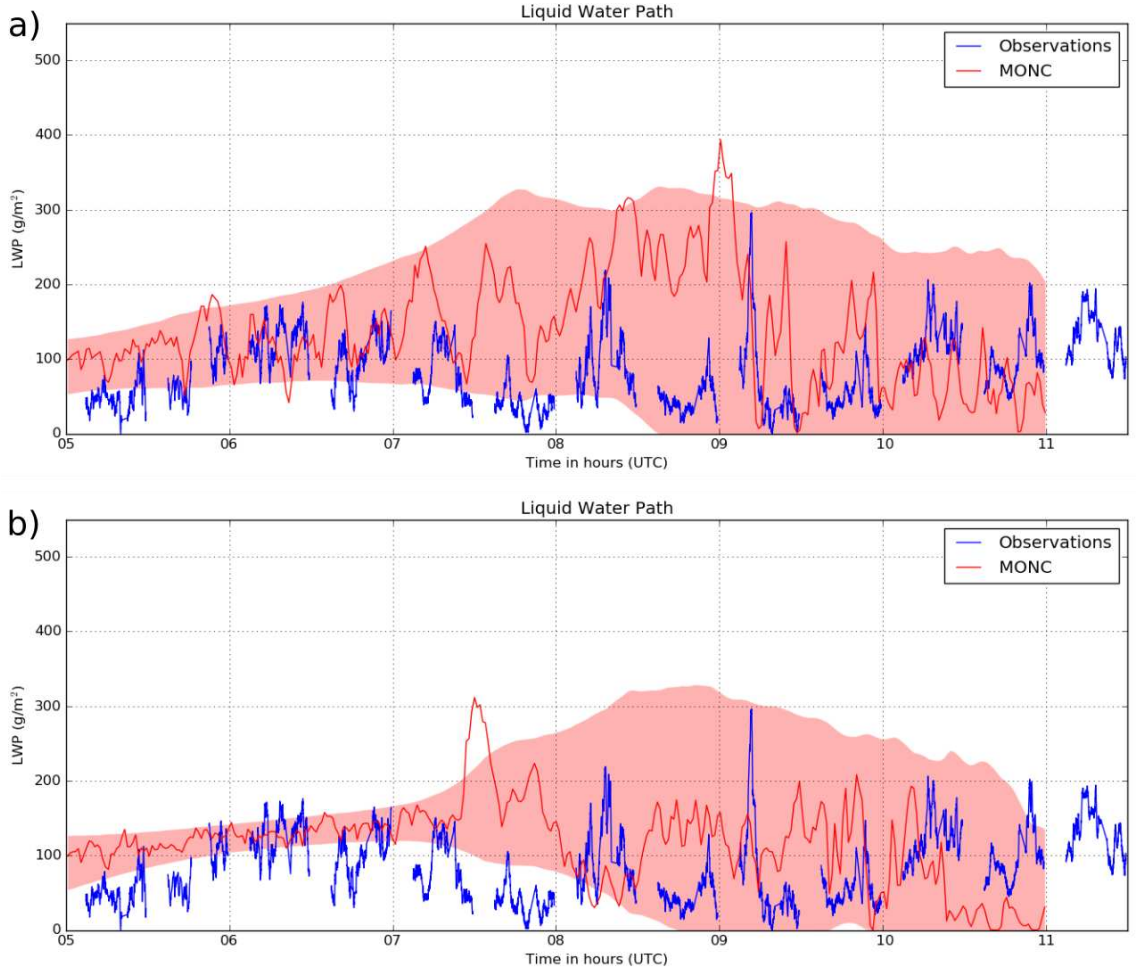

Figure 8. a) Comparison of LWP timeseries at Savé from 5 July 2016 (blue) as measured by the microwave radiometer (Wieser et al., 2016), with simulated LWP from CASIM_NO_PROC, showing the evolution of LWP at the centre of the model domain (red line) and the LWP variability within the whole domain (red shading), expressed as +/- 2 standard deviations from the domain mean value. b) as a) but for CASIM_NO_SED.

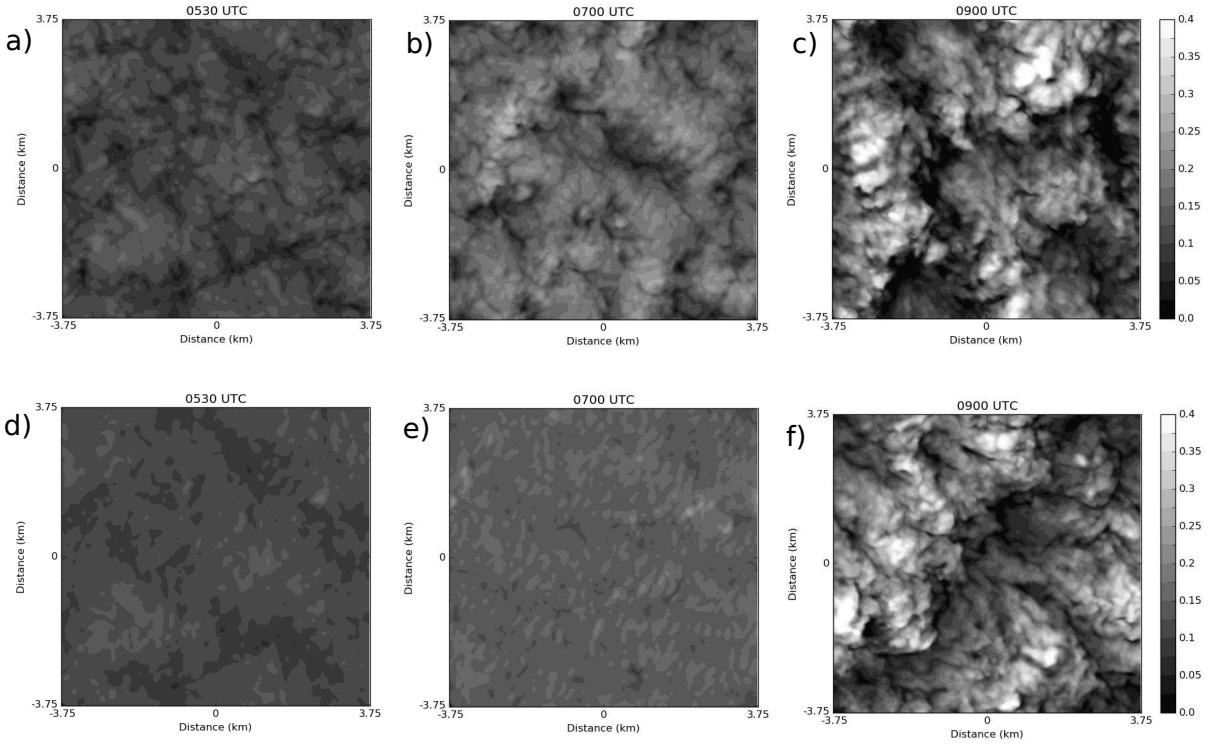

Figure 9. ~~As Fig ?? but for~~ Maps showing the ~~SIMPLE~~spatial distribution of LWP (kg m^{-2}) within the model domain at 0530, 0700 and 0900 UTC for CASIM_~~CLOUD experiment~~NO_PROC (a-c; top row) and CASIM_NO_SED (d-f; bottom row).

~~Maps showing the spatial distribution of LWP (kg m^{-2}) within the model domain at 0530, 0700 and 0900 UTC for CASIM_NO_PROC (a-c; top row) and SIMPLE_CLOUD (d-f; bottom row).~~

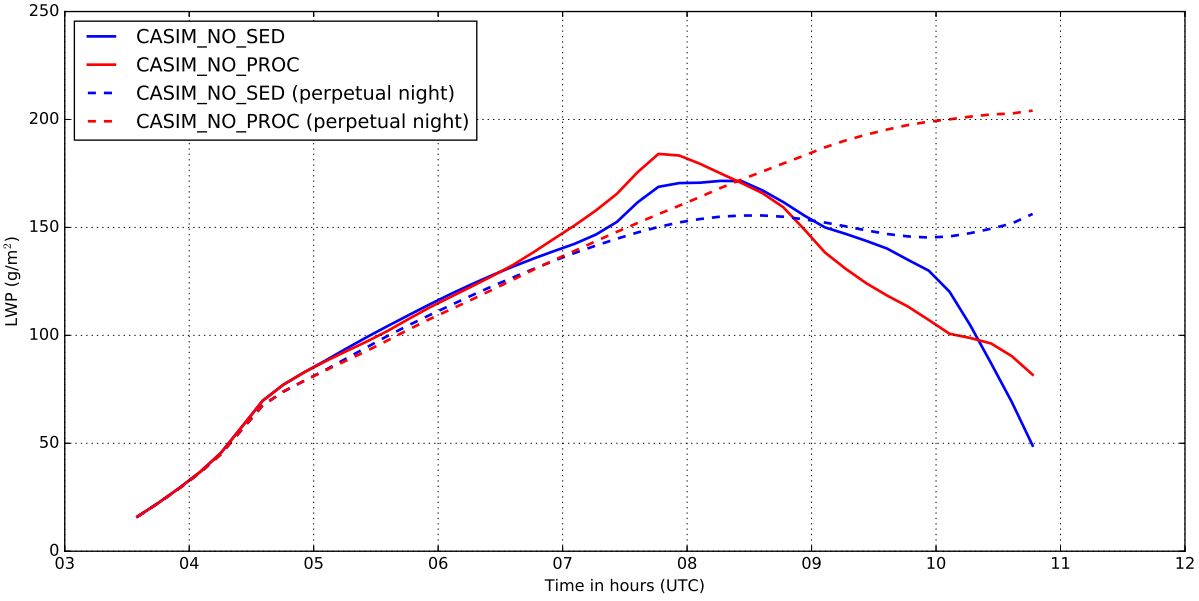

Figure 10. Timeseries of simulated LWP (g m^{-2}) from CASIM_NO_PROC (solid red line) and ~~SIMPLE~~CASIM_~~CLOUD~~ NO_SED (solid blue line). Dashed lines show results from 'perpetual night' simulations, i.e. with short wave radiation disabled and surface fluxes set to zero throughout the simulation period. In each case, LWP is calculated from 200 m to the top of the model domain, in order to ignore the thin fog layer near the surface that develops during the spin-up period and dissipates around 0630 UTC.

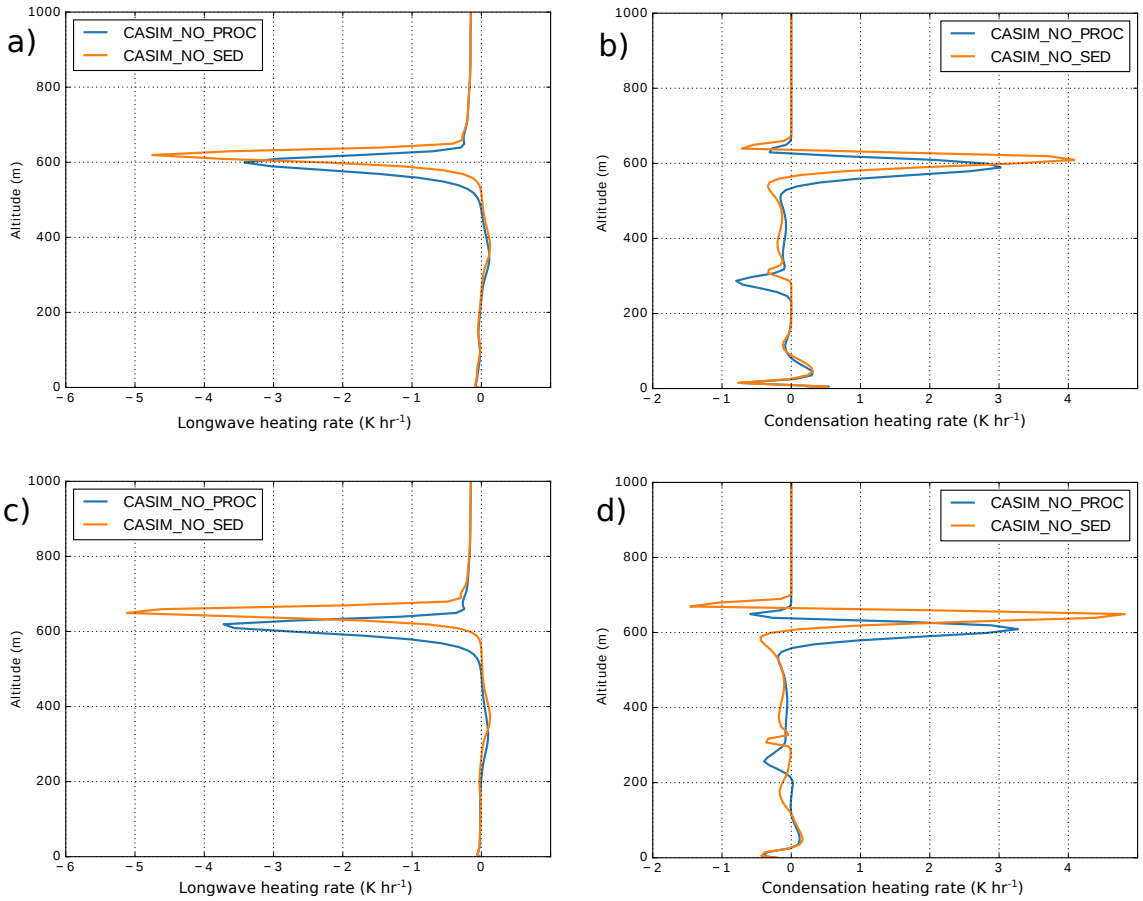

Figure 11. ~~As Fig 6 but~~ Domain average vertical profiles of a) longwave radiative heating rate (K hr^{-1}) and b) condensation heating rate (K hr^{-1}) calculated as temporal means between 0500-0530 UTC for ~~SIMPLE~~CASIM_~~CLOUD at 0530~~ NO_PROC (blue) and CASIM_NO_SED (orange). Longwave and condensation heating rates for the period 0630-0700 UTC are shown in c) and d) respectively.

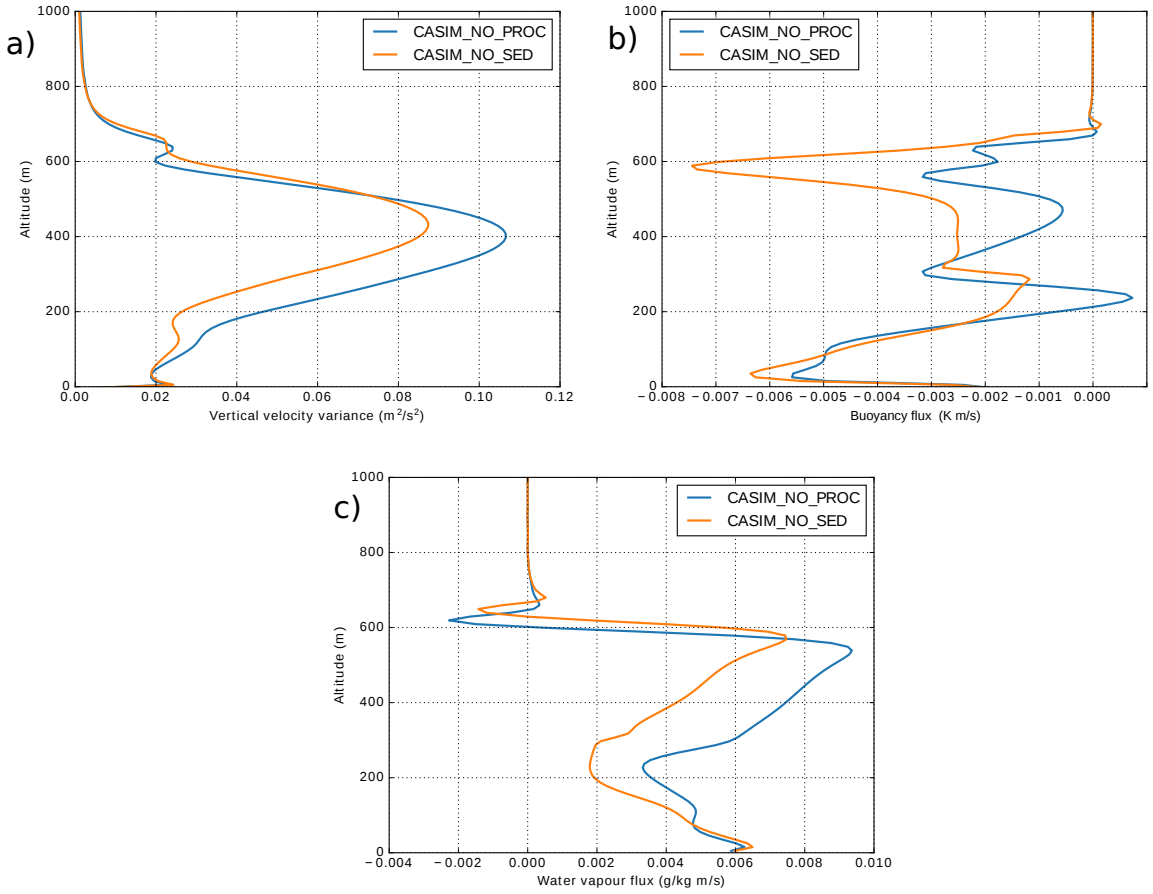

Figure 12. Domain average vertical profiles of a) vertical velocity variance (m^2 s^{-2}) b) buoyancy flux (K m s^{-1}) and c) water vapour flux (g kg^{-1} m s^{-1}), calculated as temporal means between 0530 UTC - 0700 UTC for CASIM_NO_PROC (blue) and ~~SIMPLE~~CASIM_~~CLOUD~~ NO_SED (orange).

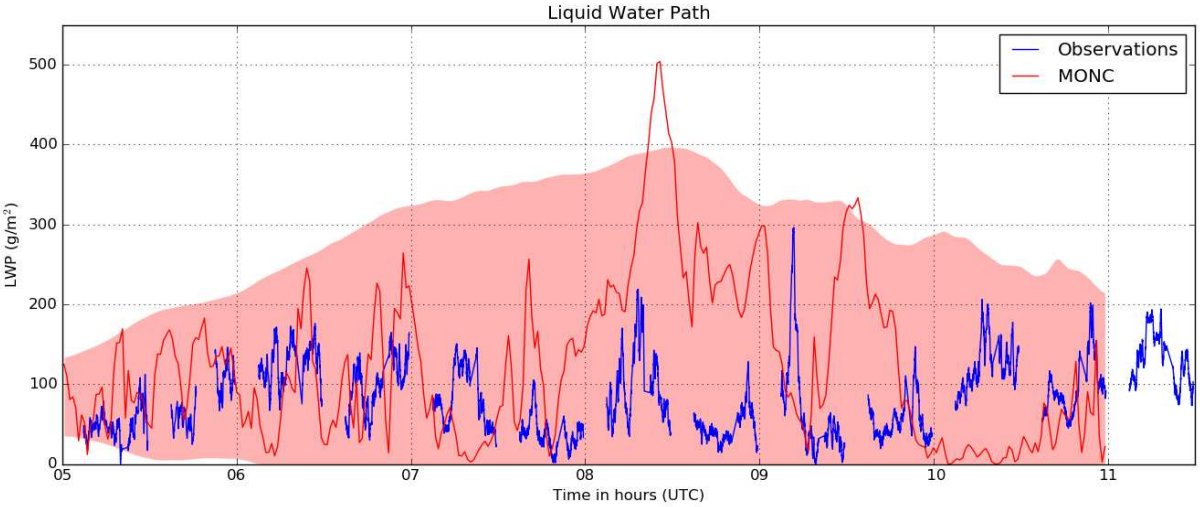

Figure 13. As Fig ~~10~~ 8 but ~~with short wave radiation disabled and surface fluxes set to zero throughout the simulation period.~~ for CASIM_200.

~~As Fig ?? but for CASIM_200.~~

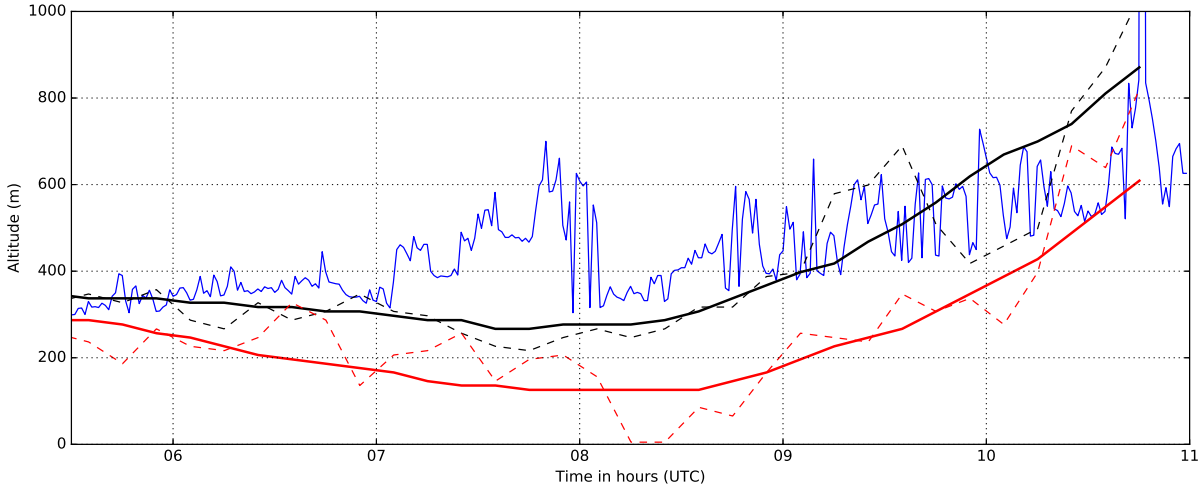

Figure 14. As Fig ~~??~~ 5b but with results from CASIM_200 ~~added (~~shown in red~~)~~.

Table 1. Table showing the mean values of liquid water path (g m^{-2}), rain water path (g m^{-2}) and surface precipitation rate (mm h^{-1}) calculated between 0600 - 0800 UTC and 0800 - 1000 UTC for five different simulations, listed in order of increasing rates of droplet sedimentation achieved by reducing droplet number.

	0600 - 0800 UTC			**0800 - 1000 UTC**		
	LWP	**RWP**	**precip rate**	**LWP**	**RWP**	**precip rate**
~~SIMPLE_CLOUD~~ CASIM_NO_SED	~~140.75~~ 143.29	0	0	~~156.66~~ 157.05	0	0
CASIM_NO_PROC	150.08	0.014	0	150.65	0.015	0
CASIM_200	133.96	0.16	0.0015	129.50	0.17	0.0017
CASIM_100	129. 49	0.24	0.004	122.47	0.33	0.0069
CASIM_50	90.58	0.44	0.025	83.29	0.59	0.015